AIMS Mathematics, 11(3): 6592–6621.
DOI:10.3934/math.2026273
Received: 04 January 2026
Revised: 17 February 2026
Accepted: 04 March 2026
Published: 16 March 2026

https://www.aimspress.com/journal/Math

Research article

Finite-time formation control with prescribed performance for multi-agent systems against FDI attacks using neural network observers

Naveed Iqbal[1,*], **Meraa Arab**[2,*], **Saba Shaheen**[3] **and Salma Trabelsi**[2]

[1] Department of Mathematics, College of Science, University of Ha'il, Ha'il 2440, Saudi Arabia
[2] Department of Mathematics and Statistics, College of Science, King Faisal University, Al Ahsa 31982, Saudi Arabia
[3] Department of Mathematics and Statistics, The University of Lahore, Sargodha 40100, Pakistan

* **Correspondence:** Email: naveediqbal1989@yahoo.com, marab@kfu.edu.sa.

Abstract: The research developed a resilient time-varying formation control strategy with prescribed-time convergence to a bounded residual set for non-strict-feedback second-order MASs to maintain accurate tracking under these conditions. Neural networks function to predict unknown nonlinear dynamics, while a state observer based on neural networks uses partial leader information to reconstruct unmeasured states. The effects of FDI attacks and communication uncertainties were addressed through matrix equalities/inequalities that solve Laplacian asymmetry problems. The proposed method achieves semi-global practical finite-time stability because it maintains all closed-loop signals within their bounded limits while tracking errors stay within their defined performance limits. The simulation results showed that formation errors achieve the prescribed bounds in finite time while maintaining stability and reliable coordination under adversarial and uncertain conditions, which demonstrates the method's robustness and scalability.

Keywords: finite-time control; multi-agent systems; FDI attack; Lyapunov function; time-varying formation control; prescribed performance control; neural network
Mathematics Subject Classification: 26A33, 34k37

1. Introduction

Multi-agent systems (MASs) have attracted much attention in the past few years and are expected to have many applications in the fields of robotics, intelligent transportation systems, aerospace systems, and autonomous vehicles. In a MAS, multiple agents interact and communicate with each other via the underlying network to accomplish tasks such as reaching consensus, achieving formation control, and cooperative tracking. The design of intelligent cyber-physical systems is a current popular and

important research topic in modern control theory, and there is an urgent need for reliable and efficient control strategies for MASs.

Advanced sensing and tracking technology is one of the key components in an intelligent control system. In [1], Du et al. proposed an automatic tracking system for a microwave deicing device applied to railway contact wire. In [2], Xu and Li proposed a predictor-based control for the system with distributed input and output delay. In [3], Guo et al. introduced an online optimization method based on Bayesian optimization for planetary rover navigation.

Cooperative motion and coordinated control have been studied extensively in the last few years. The finite-time intermittent control strategy for formation-circumnavigation switching of multiple omnidirectional intelligent navigator (ODIN) systems was proposed by Hu et al. in [4]. The worm-inspired creeping gait strategy for wheeled mobile robots with variable wheelbase control was studied by Qi et al. in [5]. Ma and Xu in [6] investigated the impact of intentional delays on consensus performance for second-order MASs and proved that with appropriate delay design, the second-order MASs can achieve better consensus performance.

In the field of control for nonlinear and uncertain systems, neural-network (NN)-based control strategies have been explored in many works. For example, in [7], Xiong and Chen introduced an RBFNN-based adaptive sliding mode controller for uncertain aerial vehicles. In [8], Zhou et al. designed a hybrid neural network and physics-based estimator for the vehicle dynamics. In [9], Luan et al. investigated a coordinated tracking control strategy for integrated wheel-end systems.

Formation control is a basic coordination problem in MASs. Recently, Chen et al. [10] proposed a range-only distributed safety-critical formation control strategy using control barrier functions and bearing estimators for safe rendezvous. Wang et al. [11] introduced an optimal event-triggered neural learning control scheme for constrained pneumatic systems to achieve more excellent control performance and energy saving. Liu et al. [12] proposed a formal multi-agent Q-learning model based on the graph structure, which is beneficial to distributed learning in collaborative systems.

Neural-network-based synchronization and control for complex nonlinear systems were also studied. Liu et al. proposed a noise-tolerant fuzzy-type zeroing neural network for robust synchronization of chaotic systems [13]. Xiong et al. investigated a recurrent neural network-based sliding mode controller for uncertain tilting quadrotor UAVs (unmanned aerial vehicles) [14]. Li et al. investigated the distributed fault-tolerant formation control for UAV swarms with the prescribed performance [15].

Recent advancements in robotics, particularly in motion planning for robotic systems and dynamic system optimization, are delivering several successful results. Optimizing the performance of intelligent autonomous systems is a key goal. Zhou et al. proposed a parallel model predictive path integral control method for high-performance obstacle avoidance of a robotic manipulator in [16]. Xu et al. summarized the transition-turbulence modeling for aerodynamic systems in [17]. Cao et al. proposed a predefined sequential synchronization control method with an event-triggered strategy for networked systems in [18].

The present paper focuses on the research of robust disturbance rejection and fault-tolerant control. In addition to the above-mentioned works, in [19], Lu et al. further proposed fixed-time disturbance rejection by means of the equivalent-input disturbance estimation method. In [20], Wang et al. focused on event-triggered adaptive predefined-time attitude tracking control for spacecraft systems. In [21], Kang et al. researched fault-tolerant control design for fuzzy stochastic systems with time-varying

delays.

Aerospace and autonomous vehicles have developed rapidly in recent years. Many new adaptive control methods have been proposed and applied in this field. In [22], Fu et al. proposed an adaptive safety attitude control strategy for the hybrid vertical take-off and landing of a UAV under multiple faults and uncertainties. Xu et al. proposed a reinforcement-learning-based steering control framework for human–machine shared driving systems under emergency obstacle avoidance conditions [23]. Yang et al. proposed a decentralized optimal fault-tolerant control for interconnected nonlinear systems using dynamic high-gain strategies in [24].

In addition to automation control, intelligent sensing and assistive technologies have also become a hot research direction in the field of cyber-physical systems. According to our literature search, Zhang et al. [25] proposed a multi-sensor fusion-based intelligent auxiliary system for power wheelchairs. Song et al. [26] investigated the velocity smoothing method for real-time curve interpolation in automated manufacturing systems. Jian and Yin [27] made reinforcement learning-based cooperative control strategies for multi-UAV systems in dense obstacle environments.

Research on the observer-based control of systems with the state variables being partially measurable is also very active. In [28], distributed prescribed-time unknown input observers were proposed for networked systems. In [29], prescribed-time observers were developed for descriptor systems with unknown inputs. In [30], the observer-based adaptive fuzzy fractional backstepping consensus control of uncertain multi-agent systems (MASs) with an event-triggered communication strategy was investigated.

Observer design is only one part of the control field. Finite-time and fixed-time control have also been popular research field. Yan et al. proposed the finite-time guaranteed cost control for uncertain stochastic systems in [31]. Hou et al. proposed a data-driven sliding mode control method for magnetorheological fluid clutch systems in [32].

Digital twin technology and the intelligent control method are developing rapidly in the era of new intelligent technology, and the autonomous system is becoming more and more complicated. Wang et al. proposed a digital-twin-driven integrated design framework for unmanned underwater vehicles in [33]. Xing et al. studied multi-UAV trajectory planning based on improved multi-agent reinforcement learning in [34]. Zheng et al. investigated hybrid nominal–robust control for hub motor systems with performance constraints in [35].

Observer-based neural control has been widely adopted in many industrial applications. Research on this topic was carried out by Yang et al. in [36], where an observer-based adaptive neural network force tracking controller was proposed for the actuator-saturation nonlinear pneumatic polishing system. Moreover, in [37], Yang et al. further extended fuzzy adaptive dynamic surface control to the contact task with uncertainties. In addition, Gu et al. investigated the event-triggered communication strategy with a large language model for UAV formation control in [38].

Apart from that, the study of intelligent perception and monitoring systems has been carried out in all the engineering fields. Lu et al. [39] explored the obstacle detection technology for autonomous electric locomotives in underground mines. Cheng et al. [40] proposed a new exponential-weighted integral inequality and analyzed the stability of time-delay systems. Li et al. [41] also explored the stability criteria for Takagi–Sugeno fuzzy systems with time-varying delays.

The papers on intelligent control systems in the fields of traffic safety and autonomous driving, achieved great success. Hou et al. [42] proposed a deep transfer learning approach for traffic conflict

prediction, Ding et al. [43] proposed a formation configuration screening method based on Poincaré contraction mapping, and Fan et al. [44] gave the fixed-time synchronization criteria for fractional-order fuzzy neural networks.

Although the MAS control field has made great progress in recent years, there are still many unsettled problems. The majority of the current control algorithms depend on the assumption of full-state measurement, and the impacts of cyber-attacks in complex distributed systems are not considered. False data injection (FDI) attacks in complex networked systems may cause great instability and performance degradation in control and coordination of multi-agent systems.

The main contributions of this paper are summarized as follows:

- A finite-time prescribed performance formation control framework is developed for second-order nonlinear multi-agent systems with partial state measurements.
- A neural-network-based observer is designed to estimate unmeasured states and unknown nonlinearities under FDI attacks.
- A resilient control law is constructed that guarantees prescribed performance and boundedness of all closed-loop signals in finite time.

1) Section 2 introduces basic graph theory alongside prescribed performance control and finite-time stability tools, as well as neural network principles, which form the basis of the proposed method.
2) Section 3 models the leader–follower MAS under FDI attacks by establishing dynamics, vulnerabilities, and control objectives.
3) Section 4 develops an adaptive NN (neural network)-based observer and sliding mode control law that provides finite-time performance and resilience.
4) In Section 5, the proposed framework is validated through simulations, which show robust and attack-resilient formation control.
5) In Section 6, the conclusion demonstrates that the FDI-resilient formation control maintains its stability and robustness.

2. Preliminaries

2.1. Graph theory

A directed graph $\mathcal{G} = \{\mathcal{V}, \mathcal{E}\}$ consists of two main components: $\mathcal{V} = \{1, 2, 3, \ldots, M\}$ represents the set of nodes (agents), and $\mathcal{E} \subseteq \mathcal{V} \times \mathcal{V}$ represents the set of directed edges that show communication links between agents. The presence of an edge $(m, n) \in \mathcal{E}$ signifies that agent n possesses the ability to transmit information to agent m.

The adjacency matrix of the graph is denoted by $\mathcal{A} = [e_{mn}] \in \mathbb{R}^{M\times M}$, where $e_{mn} = 1$ if $(m, n) \in \mathcal{E}$ and $e_{mn} = 0$ otherwise. The set of neighbors of agent m is denoted by M_m. The degree matrix $\mathcal{D}$ is defined as a diagonal matrix with entries $d_m = \sum_{n=1}^{M} e_{mn}$ that give the in-degree of each node.

Define the normalized adjacency matrix $\bar{\mathcal{A}} = [\bar{e}_{mn}] \in \mathbb{R}^{M\times M}$, where $\bar{e}_{mn} = \begin{cases} \dfrac{e_{mn}}{\sum_{k=1}^{M} e_{mk}}, & \text{if in-degree } d_m \neq 0, \\ e_{mn}, & \text{otherwise.} \end{cases}$ The normalization degree matrix is denoted by $\bar{\mathcal{D}} = \text{diag}(\bar{d}_m)$, where $\bar{d}_m = \begin{cases} 1, & \text{if } d_m \neq 0, \\ 0, & \text{if } d_m = 0. \end{cases}$ The Laplacian matrix associated with this normalized graph is given

as $\mathcal{L} = \bar{\mathcal{D}} - \bar{\mathcal{A}}$. Assume $1, \ldots, M$ function as intelligent units in the network. This designation is valid only if $d_m = 0$. Define a diagonal matrix $C = \text{diag}(c_m)$, where $c_m = \begin{cases} 0, & \text{if } d_m \neq 0, \\ 1, & \text{if } d_m = 0. \end{cases}$

Remark 2.1. Agent m operates as a follower when it receives input from at least one neighboring agent to satisfy $\sum_{n=1}^{M} \bar{e}_{mn} = 1 \quad \text{and} \quad c_m = 0$. Agent m functions as a leader when it has no incoming edges because $\sum_{n=1}^{M} \bar{e}_{mn} = 0 \quad \text{and} \quad c_m = 1$.

2.2. Prescribed performance control

Definition 2.1. A function $\rho(t)$ is called a finite-time prescribed performance function (FTPPF) if it satisfies the following properties:

1) $\rho(t) > 0, \ \forall t \geq 0$.
2) $\rho(t)$ is continuous and continuously differentiable on $[0, T_\phi)$.
3) $\rho(t)$ is strictly decreasing on $[0, T_\phi)$ and reaches a constant steady-state value in finite time, i.e., $\rho(t) = \rho_\infty, \ \forall t \geq T_\phi$.

A typical finite-time prescribed performance function is defined as in Eq (2.1).

$$\rho(t) = \begin{cases} (\rho_0 - \rho_\infty)\left(1 - \dfrac{t}{T_\phi}\right)^{\kappa} + \rho_\infty, & t < T_\phi, \\ \rho_\infty, & t \geq T_\phi. \end{cases} \tag{2.1}$$

This type of function defines a constraint boundary within which the system error must evolve. A typical finite-time performance function (FTPF), as originally introduced in [38].

Remark 2.2. *In this work, the false data injection (FDI) signal $\omega_m(t)$ is assumed to act on the local actuation channel of agent m. The modeling decision represents an actuator-side spoofing or insider attack, which causes the corrupted input to impact both the physical agent dynamics and the observer running on the local system with equal effect. The FDI signal, which enters both systems, allows them to cancel out each other in the observer error dynamics. FDI attacks on inter-agent communication channels (e.g., relative position or velocity measurements) are not considered in this study and will be investigated in future work.*

2.3. Finite-time stability analysis for dynamical systems

The theoretical background on finite-time stability, together with several important lemmas, is given as:

Definition 2.2. [37, 38] The system is described by the state vector s

$$\dot{s}(t) = \phi(t, s) + \omega_m^a(t), \quad s(0) = s_0, \tag{2.2}$$

where $\phi(t, s)$ represent a continuous nonlinear function. A false data injection (FDI) signal denoted by $\omega_m^a(t)$ is introduced by a malicious agent. The signal $\omega_m^a(t)$ represents a bounded false data injection (FDI) attack vector that malicious agents create to enter the system dynamics as a matched disturbance.

Equation (2.2) is said to be semi-globally practically finite-time (SGPF) stable if there exists a finite time $\mathcal{T}(s_0)$, such that $\|s(t)\| \leq \delta, \ t \geq \mathcal{T}$, and δ is a prescribed positive constant.

Lemma 2.3. *[39]* Let φ_1 and φ_2 be positive constants, $\varphi_1 > 0$, and $0 < \varphi_2 < 1$. The following condition is satisfied for a smooth and positive definite function $\mathcal{V}(s)$:

$$\dot{\mathcal{V}}(s) + \varphi_1 \mathcal{V}^{\varphi_2}(s) \leq 0.$$

The system demonstrates finite-time convergence through a duration that depends on its initial state s_0 according to the system $\mathcal{T}(s_0) \leq \frac{\mathcal{V}(s_0)^{1-\varphi_2}}{\varphi_1(1-\varphi_2)}$.

Lemma 2.4. *For any $a, b \geq 0$ and $p, q > 1$ satisfying $\frac{1}{p} + \frac{1}{q} = 1$, young's inequality holds: $ab \leq \frac{a^p}{p} + \frac{b^q}{q}$.*

Assumption 2.1. The system keeps all agent states, observer states, and auxiliary error signals inside a compact set $\Psi_s \subset \mathbb{R}^q$. Moreover, the unknown nonlinear functions $r_{m,n}(.)$ are continuous and locally Lipschitz on Ψ_s.

Lemma 2.5. *[40]* Suppose $\tau_1 \geq 0$, $\tau_2 \geq 0$, $\tau_3 \geq 0$, $\bar{\tau} \geq 0$, $\underline{\tau} \geq 0$, and $\rho \geq 0$. Then, the following inequality holds:

$$\bar{\tau}^{\tau_1} \underline{\tau}^{\tau_2} \rho \leq \tau_3 \bar{\tau}^{\tau_1+\tau_2} + \frac{\tau_2}{\tau_1+\tau_2} \left[\frac{\tau_1}{\tau_3(\tau_1+\tau_2)} \right]^{\frac{\tau_1}{\tau_2}} \rho^{\frac{\tau_1+\tau_2}{\tau_2}} \underline{\tau}^{\tau_1+\tau_2}.$$

According to standard universal approximation results for neural networks on compact sets, the approximation error is uniformly bounded on Ψ_s.

It is noted that Lyapunov inequalities of the form $\dot{\mathcal{V}} \leq -k\mathcal{V} + c$ guarantee exponential convergence to a compact residual set, which corresponds to practical finite-time stability, rather than exact finite-time stability.

2.4. Neural networks

Neural networks demonstrate their strength through their capability to precisely approximate nonlinear functions. The unknown nonlinear function is denoted by $\phi(s) : \mathbb{R}^l \to \mathbb{R}$. A neural network can approximate this function as $\phi(s) = \beta^{\mathcal{T}} \varepsilon(s)$, where $s \in \Psi_s \subset \mathbb{R}^q$ is the input vector, $\beta = [\underline{p}_1, \underline{p}_2, \ldots, \underline{p}_q]^{\mathcal{T}} \in \mathbb{R}^q$ denotes the adjustable weight vector, and $\varepsilon(s) = [\underline{\varepsilon}_1(s), \underline{\varepsilon}_2(s), \ldots, \underline{\varepsilon}_q(s)]^{\mathcal{T}}$ is a vector of basis functions. The Gaussian function serves as a common basis function in the radial basis function as $\underline{\varepsilon}_m(s) = \exp\left(-\frac{(s-N_m)^{\mathcal{T}}(s-N_m)}{2c_m^2}\right)$.

The mth neuron has a Gaussian distribution with center $N_m = [N_{m1}, N_{m2}, \ldots, N_{mq}]$ and width parameter $c_m > 0$.

Lemma 2.6. *[41]* Any continuous function $\phi(s)$ defined on a compact set Ψ_s has a neural network approximation $\phi(s) = \beta^{*\mathcal{T}} * \varepsilon(s) + \zeta$. The optimal weight vector is denoted by β^*, and ζ represents the minimum approximation error that results from this ideal configuration. The value ζ minimizes the approximation deviation in the supremum norm, expressed as

$$\beta^* = \arg\min_{\beta \in Z^q} \left\{ \sup \left\| \phi(s) - \beta^{\mathcal{T}} \varepsilon(s) \right\| \right\}.$$

3. System modeling and control framework

3.1. Attack model

The adversary introduces the false data injection (FDI) signal at agent h, denoted by $\omega_m^a(t)$, which has the following conditions:

$$\omega_m^a(t) = \begin{cases} \varsigma(t), & \text{if } h \in \mathcal{B}, \\ 0, & \text{if } h \notin \mathcal{B}. \end{cases} \tag{3.1}$$

The adversarial input strategy in the Laplace domain is defined by $\varsigma(t) \in \mathbb{R}^v$ while $\mathcal{B} \subseteq \{1, \ldots, M\}$ represents the compromised agents. The agent's state vectors $\mathbb{R}^v$ expand the attack surface of the system dynamics because they increase the dimensionality of the agent's state vectors. The injected signal affects the agent dynamics in the same manner as the nominal control input. The attack is locally injected and does not corrupt inter-agent communication signals.

4. System problem definition and proposed control approach

4.1. Dynamics of the multi-agent system

A networked multi-agent system (MAS) comprises M agents operating under non-strict feedback dynamics with unknown nonlinearities and partially unmeasurable states. The dynamics of the *mth* follower are described as follows:

$$\begin{cases} \dot{s}_{m,0} = s_{m,1} + r_{m,1}\left(\underline{s}_m\right), \\ \dot{s}_{m,1} = r_{m,2}\left(\underline{s}_m\right) + \mu_m + \omega_m^a(t), \\ w_m = s_{m,0}. \end{cases} \tag{4.1}$$

Here, $s_{m,0} \in \mathbb{R}^v$ denotes the initial value of the output state, and therefore $w_m(t) \in \mathbb{R}^v$ for all $t \geq 0$. The state vector is defined as $\underline{s}_m = \begin{bmatrix} s_{m,0}^{\mathcal{T}} & s_{m,1}^{\mathcal{T}} \end{bmatrix}^{\mathcal{T}} \in \mathbb{R}^{2v}$, where each state component satisfies $s_{m,n} \in \mathbb{R}^v$ for $n = (1, 2)$. The nonlinear mappings are unknown and capture the system's dynamics $r_{m,n}(\underline{s}_m) \in \mathbb{R}^v$. The control input μ_m is a design element of the distributed controller.

The FDI signal, which an adversary injects into the control channel, is denoted by $\omega_m^a(t)$. $w_m \in \mathbb{R}^v$ denotes the system output, where only the positional part of the state can be locally observed. This formulation represents the system with partial state observability and uncertain nonlinear behavior. The second-order nonlinear system represents the behavior of the leader.

$$\begin{cases} \dot{s}_{0,0} = s_{0,1}, \\ \dot{s}_{0,1} = r_{0,0}\left(s_{0,0}, s_{0,1}\right), \end{cases} \tag{4.2}$$

where $s_{0,0} \in \mathbb{R}^v$ is the measurable position and $r_{0,0}(s_{0,0}, s_{0,1})$ is a smooth, predefined nonlinear function. The analysis and control of the system assumes that the trajectory and its time derivatives are uniformly bounded by known constants $\left\|s_{0,0}^{(n)}\right\| \leq \bar{s}_n$, for $n = (1, 2)$. The transformation enables the conversion of system (4.1) into an equivalent dynamic representation.

$$\begin{cases} \dot{s}_{m,0} = s_{m,1} + r_{m,1}\left(\hat{\underline{s}}_m\right) + \delta\mathcal{G}_{m,1}, \\ \dot{s}_{m,1} = r_{m,2}\left(\hat{\underline{s}}_m\right) + \mu_m + \omega_m^a(t) + \delta\mathcal{G}_{m,2}, \\ w_m = s_{m,0}, \end{cases} \tag{4.3}$$

where $\hat{s}_m$ denotes the estimated state generated by the neural network observer defined in Eq (4.7). The unknown function $\underline{\hat{s}}_m = \begin{bmatrix} \hat{s}_{m,0}^{\mathcal{T}} & \hat{s}_{m,1}^{\mathcal{T}} \end{bmatrix}^{\mathcal{T}} \in \mathbb{R}^{2v}$, $\delta\mathcal{G}_{m,1} = r_{m,1}(\underline{s}_m) - r_{m,1}(\underline{\hat{s}}_m)$, $\delta\mathcal{G}_{m,2} = r_{m,2}(\underline{s}_m) - r_{m,2}(\underline{\hat{s}}_m)$. $\underline{\hat{s}}_m$ is approximated by the estimate $\underline{s}_m$, which is derived through a neural network observer. The attack signal $\omega_m^a(t)$ disrupts the estimated model, leading to trajectory deviation and reduced observer accuracy.

Assumption 4.1. The unknown nonlinear functions in Eqs (4.1) and (4.3) are locally Lipschitz continuous on a compact set containing the closed-loop trajectories. Moreover, the neural network approximation errors in Eq (4.8) are uniformly bounded. These assumptions guarantee the validity of the Lyapunov-based stability analysis in Eqs (4.25) and (4.28).

The FDI attack is modeled as an additive disturbance on the actuator channel. With this approximation, Eq (4.3) can be rewritten as:

$$\begin{cases} \dot{\underline{s}}_m = (\mathcal{A}_m \otimes \mathcal{I}_v)\underline{s}_m + \sum_{n=1}^{2}(C_{m,n} \otimes r_{m,n}(\underline{\hat{s}}_m)) \\ \qquad\quad + \delta\mathcal{G}_m + (\Upsilon_m \otimes (\mu_m + \omega_m^a)), \\ w_m = (N_m^{\mathcal{T}} \otimes \mathcal{I}_v)\underline{s}_m. \end{cases} \tag{4.4}$$

The definition of $s_m = [\, s_{m,1}^{\top},\ s_{m,2}^{\top}\,]^{\top} \in \mathbb{R}^{2v}$, in the augmented state, maintains the same dimensions as $A_m \otimes I_v \in \mathbb{R}^{2v\times 2v}$, where $\mathcal{A}_m = \begin{bmatrix} -y_{m,1} & 1 \\ -y_{m,2} & 0 \end{bmatrix}$, $C_{m,1} = \begin{bmatrix} 1 \\ 0 \end{bmatrix}$, $C_{m,2} = \begin{bmatrix} 0 \\ 1 \end{bmatrix}$, $\Upsilon_m = \begin{bmatrix} 0 \\ 1 \end{bmatrix}$, $N_m = \begin{bmatrix} 1 \\ 0 \end{bmatrix}$, $\delta\mathcal{G}_m = \begin{bmatrix} \delta\mathcal{G}_{m,1} \\ \delta\mathcal{G}_{m,2} \end{bmatrix}$, $\omega_m^a = \begin{bmatrix} \omega_1^a \\ \omega_2^a \end{bmatrix}$.

The components of $y_{m,n}$ can be selected to ensure that the matrix $\mathcal{A}_m$ is strictly Hurwitz. There exists a symmetric positive definite matrix R_m satisfying

$$\mathcal{A}_m^{\mathcal{T}} R_m + R_m \mathcal{A}_m = -S_m. \tag{4.5}$$

S_m is a designer-specified symmetric positive definite matrix, selected to ensure the existence of a unique positive definite solution R_m to the Lyapunov equation.

The FDI signal ω_m^a enters agent m through Υ_m, which modifies its behavior and may cause system coordination problems.

Definition 4.1. The following condition needs to be satisfied to achieve finite-time prescribed performance formation control for multi-agent systems (MASs).

$$\left\| \underline{s}_m(t) - \underline{s}_0(t) - l_m(t) \right\| \le \theta_{b_{m_{\mathcal{T}_\phi}}}, \quad t \ge \mathcal{T}_\phi. \tag{4.6}$$

Throughout this paper, $\|\cdot\|$ denotes the standard Euclidean norm, where $\mathcal{T}_\phi$ is a predetermined finite convergence time, and $l_m = [l_{m,0}^{\mathcal{T}}, l_{m,1}^{\mathcal{T}}]^{\mathcal{T}}$ is the time-varying formation between the leader and the mth follower. The function $\theta_{b_{m_{\mathcal{T}_\phi}}}$ defines the performance bound to be satisfied at time $\mathcal{T}_\phi$.

Remark 4.1. *MASs can achieve time-varying formation if the condition $\dot{l}_{m,0}(t) = l_{m,1}(t)$ is met. Also, to maintain a stable formation, both the reference trajectory and its first two derivatives must be bounded by a constant $\bar{l}_n$.*

Remark 4.2. *Swarm coordination strategies use time-varying inter-agent spacing because formation geometry changes through modifications of heading or tracking paths. The control system maintains a dynamic formation configuration through the non-zero constant formation offset vector l_m. The system reduces to a leader-follower tracking model when $l_m = 0$ in Eq (4.6) because agents track the leader's trajectory. Time-varying formation control includes both formation maintenance and consensus tracking as specific instances of its functionality. The formation tracking error can be defined as:*

$$\begin{cases} b_{m,0}(t) = s_{m,0} - s_{0,0} - l_{m,0}(t), \\ b_{m,1}(t) = s_{m,1} - s_{0,1} - l_{m,1}(t), \end{cases}$$

where $b_{m,0}(t)$ and $b_{m,1}(t)$ denote the tracking deviations in position and velocity, respectively, for the desired time-varying formation offsets. The system achieves semi-global practical finite-time stability because all tracking errors will reach a small area near the origin within a specific limited time period.

Objective of the control scheme: The control system achieves finite-time prescribed performance-based time-varying formation for second-order MASs with unknown nonlinearities, Eqs (4.1) and (4.2), and unobservable states. This is achieved through using an adaptive neural network observer to estimate unmeasured states and compensating for unknown dynamics, as well as by developing a control law that combines sliding mode control (SMC) with finite-time performance functions to achieve convergence within a specified time frame.

4.2. State observation for nonlinear systems via neural networks

The estimation of unobservable states in systems with unknown nonlinearities requires the use of neural network observers in the following manner:

$$\begin{cases} \dot{\hat{s}}_{m,0} = \hat{s}_{m,1} + \hat{r}_{m,1}\left(\underline{\hat{s}}_m\right) + y_{m,1}\left(w_m - \hat{w}_m\right), \\ \dot{\hat{s}}_{m,1} = \hat{r}_{m,2}\left(\underline{\hat{s}}_m\right) + \mu_m + \omega_m^a(t) + y_{m,2}\left(w_m - \hat{w}_m\right), \\ \hat{w}_m = \hat{s}_{m,0}. \end{cases} \tag{4.7}$$

Equation (4.7) defines the dynamic evolution of the observer state estimate $\hat{s}_{m,0}$, which is necessary for deriving the observer error dynamics in Eq (4.9).

The implementation does not use the unknown attack signal, which is represented by $\omega_m^a(t)$ because it remains unmeasurable. The system employs an online neural network observer, which serves as a protective mechanism to predict its operational behavior against FDI attacks.

The unknown nonlinear mapping $\hat{r}_{m,n}(\cdot)$ from (4.3) is approximated by $r_{m,n}(\cdot)$ using a neural network, denoted as:

$$\begin{cases} \hat{r}_{m,1}\left(\underline{\hat{s}}_m\right) = \hat{\beta}_{m,1}^{\mathcal{T}} \varepsilon_{m,1}(\underline{\hat{s}}_m), \\ \hat{r}_{m,2}\left(\underline{\hat{s}}_m\right) = \hat{\beta}_{m,2}^{\mathcal{T}} \varepsilon_{m,2}(\underline{\hat{s}}_m). \end{cases} \tag{4.8}$$

Here, $\hat{\beta}_{m,n}$ denotes the adjustable neural network weight vector associated with the basis function $\varepsilon_{m,n}(\underline{\hat{s}}_m)$. The neural network-based approximations produce errors that are given as follows:

$$\begin{cases} \zeta_{m,1} = r_{m,1}(\underline{s}_m) - \hat{r}_{m,1}(\underline{\hat{s}}_m), \\ \zeta_{m,2} = r_{m,2}(\underline{s}_m) - \hat{r}_{m,2}(\underline{\hat{s}}_m). \end{cases}$$

The associated approximation error $\zeta_{m,n}$ adheres to the bound $\left|\zeta_{m,n}\right| < \bar{\zeta}_{m,n}$, where $\bar{\zeta}_{m,n}$ is an unknown positive constant. The reformulation of Eq (4.7) follows the same pattern as the derivation in Eq (4.4).

$$\begin{cases} \dot{\hat{\underline{s}}}_m = (\mathcal{A}_m \otimes \mathcal{I}_v)\hat{\underline{s}}_m + (Y_m \otimes w_m) + (\Upsilon_m \otimes (\mu_m + \omega_m^a(t)) \\ \qquad\qquad + \sum_{n=1}^{2}(C_{m,n} \otimes \hat{r}_{m,n}(\underline{s}_m)), \\ w_m = (N_m^{\mathcal{T}} \otimes \mathcal{I}_v)\hat{\underline{s}}_m, \end{cases}$$

where $Y_m = [y_{m,1}, y_{m,2}]^{\mathcal{T}}$. The observation error vector is represented as

$$\begin{aligned} \dot{\mathcal{E}}_m &= (\mathcal{A}_m \otimes \mathcal{I}_v)\mathcal{E}_m \\ &\quad + \sum_{n=1}^{2}(C_{m,n} \otimes (r_{m,n}(\hat{\underline{s}}_m) - \hat{r}_{m,n}(\hat{\underline{s}}_m))) \\ &= (\mathcal{A}_m \otimes \mathcal{I}_v)\mathcal{E}_m + \zeta_m. \end{aligned} \tag{4.9}$$

$\mathcal{E}_m = \begin{bmatrix}\mathcal{E}_{m,0} & \mathcal{E}_{m,1}\end{bmatrix}^{\mathcal{T}}$, in which $\mathcal{E}_{m,0} = w_m - \hat{w}_m$ and $\mathcal{E}_{m,1} = s_{m,1} - \hat{s}_{m,1}$. The neural network estimation error is denoted by $\zeta_m = \begin{bmatrix}\zeta_{m,1}^{\mathcal{T}} & \zeta_{m,2}^{\mathcal{T}}\end{bmatrix}^{\mathcal{T}}$ and satisfies the constraint $\|\zeta_m\| \leq \bar{\zeta}_m$, where $\bar{\zeta}_m$ is an unknown but positive scalar.

It is assumed that the false data injection (FDI) attack enters both the plant and the observer through the same matched channel, as the observer relies on corrupted measurements or communicated data. Under this matched attack structure, the attack terms cancel in the observer error dynamics, yielding Eq (4.9). The design of resilient observer-based control systems relies on these standard assumptions. The FDI signal produces identical effects on both the plant and observer system under actuator-side attack conditions described in Remark 2.2, which results in observer error dynamics Eq (4.9) becoming zero; this phenomenon does not occur when communication channels are under attack. The system stability remains ensured when the nominal error dynamics are asymptotically stable because the FDI attack affects both the system and observer uniformly.

Theorem 4.3. *The neural network observer defined in (4.7) operates under the condition that*

$$\dot{\hat{\beta}}_{m,n} = \Xi_{m,n}\left[(\mathcal{E}_{m,0}N_m^{\mathcal{T}}Y_m^{-1})\varepsilon_{m,n}(\hat{\underline{s}}_m)\right] - \alpha_{m,n}\hat{\beta}_{m,n}. \tag{4.10}$$

The matrix Y_m is a diagonal positive definite observer gain matrix and is therefore invertible. And $\Xi_{m,n} = \Xi_{m,n}^{\mathcal{T}} > 0$ and the adaptation gain $\alpha_{m,n}$ satisfies $\alpha_{m,n} > \frac{1}{2}\|N_m^{\mathcal{T}}Y_m^{-1}\|^2$ for each agent m. The state observation error $\mathcal{E}_m$ and the NN parameter estimation error $\hat{\beta}_{m,n}$ remain uniformly ultimately bounded. Furthermore, the observation error norm is constrained by $\|\mathcal{E}_m\| \leq \bar{\mathcal{E}}_m$, where $\bar{\mathcal{E}}_m$ denotes a positive constant.

Proof. The stability analysis is based on a suitable Lyapunov function

$$\mathcal{V}_1 = \frac{1}{2}\sum_{m=1}^{M}\mathcal{E}_m^{\mathcal{T}}(R_m \otimes \mathcal{I}_v)\mathcal{E}_m + \frac{1}{2}\sum_{m=1}^{M}\sum_{n=1}^{2}\tilde{\beta}_{m,n}^{\mathcal{T}}\Xi_{m,n}^{-1}\tilde{\beta}_{m,n}, \tag{4.11}$$

where $\tilde{\beta}^{\mathcal{T}}_{m,n} = \beta^{*}_{m,n} - \hat{\beta}^{\mathcal{T}}_{m,n}$. Let $\beta^{*}_{m,n}$ denote the ideal neural network weight vector that minimizes the approximation error of the unknown nonlinear function $r_{m,n}$ over a compact set, as defined in Lemma 2.6.

The derivative of the function results in the expression shown in Eq (4.11) by using Eqs (4.9) and (4.10).

$$\begin{aligned}
\dot{\mathcal{V}}_1 &= \frac{1}{2}\sum_{m=1}^{M}\left[\mathcal{E}_m^{\mathcal{T}}(\mathcal{A}_m^{\mathcal{T}}R_m \otimes \mathcal{I}_v)\mathcal{E}_m + \mathcal{E}_m^{\mathcal{T}}(R_m\mathcal{A}_m \otimes \mathcal{I}_v)\mathcal{E}_m\right] \\
&\quad + \sum_{m=1}^{M}\mathcal{E}_m^{\mathcal{T}}(R_m \otimes \mathcal{I}_v)\zeta_m - \sum_{m=1}^{M}\sum_{n=1}^{2}\tilde{\beta}^{\mathcal{T}}_{m,n}\Xi^{-1}_{m,n}\dot{\hat{\beta}}_{m,n} \\
&= \sum_{m=1}^{M}\left[-\mathcal{E}_m^{\mathcal{T}}(S_m \otimes \mathcal{I}_v)\mathcal{E}_m + \mathcal{E}_m^{\mathcal{T}}(R_m \otimes \mathcal{I}_v)\zeta_m\right] \\
&\quad - \sum_{m=1}^{M}\sum_{n=1}^{2}\tilde{\beta}^{\mathcal{T}}_{m,n}\left[(\mathcal{E}_{m,0}N_m^{\mathcal{T}}Y_m^{-1})\varepsilon_{m,n}(\hat{s}_m) - \tilde{\beta}^{\mathcal{T}}_{m,n}\alpha_{m,n}\hat{\beta}_{m,n}\right] \\
&\leq \sum_{m=1}^{M}\left[-\mathcal{E}_m^{\mathcal{T}}(S_m \otimes \mathcal{I}_v)\mathcal{E}_m + \mathcal{E}_m^{\mathcal{T}}(R_m \otimes \mathcal{I}_v)\zeta_m\right] \\
&\quad + \sum_{m=1}^{M}2\|\mathcal{E}_m\|^2 + \frac{1}{2}\sum_{m=1}^{M}\sum_{n=1}^{2}\left[\frac{1}{2}\left(\|N_m^{\mathcal{T}}Y_m^{-1}\|\|\tilde{\beta}^{\mathcal{T}}_{m,n}\|\right)^2 + \alpha_{m,n}\|\beta^{*}_{m,n}\|^2 - \alpha_{m,n}\|\tilde{\beta}_{m,n}\|^2\right].
\end{aligned} \tag{4.12}$$

The neural network approximation error satisfies $\|\zeta_m\| \leq \bar{\zeta}_m$, where $\bar{\zeta}_m > 0$ is an unknown positive scalar constant.

The simplified form emerges from applying Lemma (2.4) to the expression.

$$\mathcal{E}_m^{\mathcal{T}}(R_m \otimes \mathcal{I}_v)\zeta_m \leq \frac{1}{2}\|\mathcal{E}_m\|^2_{R_m} + \frac{1}{2}\|R_m \otimes \mathcal{I}_v\|^2\bar{\zeta}_m^2. \tag{4.13}$$

The reformulation of Eq (4.12) becomes possible through the combination of this expression with Eq (4.13).

$$\begin{aligned}
\dot{\mathcal{V}}_1 \leq &\sum_{m=1}^{M}\left[-\mathcal{E}_m^{\mathcal{T}}\left(\frac{1}{2}(S_m - 5\mathcal{I}_2) \otimes \mathcal{I}_v\right)\mathcal{E}_m\right] + \ell_1 \\
&- \frac{1}{2}\sum_{m=1}^{M}\sum_{n=1}^{2}\left(\alpha_{m,n} - \frac{1}{2}\|N_m^{\mathcal{T}}Y_m^{-1}\|^2\right)\Xi_{m,n}(\tilde{\beta}^{\mathcal{T}}_{m,n}\Xi^{-1}_{m,n}\tilde{\beta}_{m,n}),
\end{aligned} \tag{4.14}$$

where $\ell_1 = \frac{1}{2}\sum_{m=1}^{M}\|R_m \otimes \mathcal{I}_v\|^2\bar{\zeta}_m^2 + \frac{1}{2}\sum_{m=1}^{M}\sum_{n=1}^{2}\alpha_{m,n}\left\|\beta^{*}_{m,n}\right\|^2$.

Equation (4.14) is established as:

$$\begin{aligned}
\dot{\mathcal{V}}_1 &\leq -\frac{1}{2}\sum_{m=1}^{M}\left[\frac{2\gamma_{\min}^{\frac{1}{2}(S_m - 5\mathcal{I}_2)}}{\gamma_{\max}^{R_m}}\mathcal{E}_m^{\mathcal{T}}(R_m \otimes \mathcal{I}_v)\mathcal{E}_m\right] + \ell_1 \\
&\quad - \sum_{m=1}^{M}\sum_{n=1}^{2}\frac{2\alpha_{m,n} - \|N_m^{\mathcal{T}}Y_m^{-1}\|^2}{2\gamma_{\max}^{\Xi^{-1}_{m,n}}}(\tilde{\beta}^{\mathcal{T}}_{m,n}\Xi^{-1}_{m,n}\tilde{\beta}_{m,n}) \\
&\leq -K_1\mathcal{V}_1 + \ell_1.
\end{aligned}$$

In this context, $\gamma_{\min}^{\frac{1}{2}(S_m-5\mathcal{I}_2)}$, $\gamma_{\max}^{R_m}$, and $\gamma_{\max}^{\Xi_{m,n}^{-1}}$ represent the minimum singular value of $\frac{1}{2}(S_m - 5\mathcal{I}_2)$, the maximum singular value of R_m, and the maximum singular value of $\Xi_{m,n}^{-1}$, respectively. In addition, $K_1 = \min_{1\le m\le M}\left\{\frac{\gamma_{\min}^{\frac{1}{2}(S_m-5\mathcal{I}_2)}}{\gamma_{\max}^{R_m}}, \frac{2\alpha_{m,n}-\left\|N_m^{\mathcal{T}}Y_m^{-1}\right\|^2}{2\gamma_{\max}^{\Xi_{m,n}^{-1}}}\right\}$. The theoretical analysis shows that the observation error $\mathcal{E}_m$ and the estimated neural network weight $\hat{\beta}_{m,n}$ are guaranteed to be uniformly ultimately bounded (UUB) when the given condition is satisfied,

$$K_1 > 0. \tag{4.15}$$

The boundedness result applies when the FDI attack impacts the local actuation channel, and the observer receives the same information as the attack, which enables the observer to cancel the attack in the estimation error system.

From Lyapunov stability analysis, all closed-loop signals are bounded and converge in finite time. Therefore, the system trajectories remain inside a compact invariant set Ψ_s. This ensures the validity of the neural network approximation on Ψ_s.

Remark 4.4. *The term $S_m - 5I_2$ is introduced to guarantee the strict negative definiteness of the resulting matrix expression in the Lyapunov derivative. Specifically, S_m is a symmetric positive definite adaptive gain matrix. Subtracting $5I_2$ enforces $S_m - 5I_2 \prec 0$ whenever the minimum eigenvalue S_m is upper-bounded by 5.*

The design parameter 5 serves as a constant that maintains strict negative definiteness $S_m - 5I_2$ to handle both bounded neural approximation and disturbance terms. □

4.3. Formulation of the control law

The MASs, represented by Eqs (4.1) and (4.2), achieve effective FTPPC through the observer design in (4.7) and the adaptive learning law in (4.11). The first step involves establishing time-dependent estimation errors:

$$\begin{cases}\hat{b}_{m,0}(t) = \hat{s}_{m,0} - s_{0,0} - l_{m,0}(t),\\ \hat{b}_{m,1}(t) = \hat{s}_{m,1} - s_{0,1} - l_{m,1}(t).\end{cases} \tag{4.16}$$

It is assumed that the leader's position $s_{0,0}$ is available to all follower agents through direct communication or broadcast. The derivation of estimation error for time-varying MASs formation control is concluded from Eq (4.16):

$$\begin{cases}\dot{\hat{b}}_{m,0}(t) = \dot{\hat{s}}_{m,0} - \dot{s}_{0,0} - \dot{l}_{m,0}(t),\\ \dot{\hat{b}}_{m,1}(t) = \dot{\hat{s}}_{m,1} - \dot{s}_{0,1} - \dot{l}_{m,1}(t).\end{cases}$$

The estimation error for time-varying formation control of the MAS is defined as follows:

$$\begin{aligned}\hat{\epsilon}_{m,\tau} &= \sum_{n\in\mathcal{N}_m}\bar{a}_{mn}\left(\hat{s}_{m,\tau} - l_{m,\tau} - \hat{s}_{n,\tau} + l_{n,\tau}\right)\\ &\quad + c_m\left(\hat{s}_{m,\tau} - s_{0,\tau} - l_{m,\tau}\right)\\ &= \sum_{n\in\mathcal{N}_m}\bar{a}_{mn}\left(\hat{s}_{m,\tau} - \hat{s}_{n,\tau}\right) + c_m\left(\hat{s}_{m,\tau} - s_{0,\tau}\right)\\ &\quad + \sum_{n\in\mathcal{N}_m}\bar{a}_{mn}\left(-l_{m,\tau} + l_{n,\tau}\right) + c_m\left(-l_{m,\tau}\right).\end{aligned} \tag{4.17}$$

Here, $\mathcal{N}_m$ denotes the neighbor set of agent m, and a_{mn} are elements of the adjacency matrix associated with the communication graph.

Equation (4.17) can be written as follows:

$$\hat{\epsilon}_\tau = (\mathcal{L} + C) \otimes \mathcal{I}_v \cdot (\hat{s}_\tau - \mathbf{1}_M \otimes s_{0,\tau}) + \hbar_\tau.$$

Here, $\hbar_{m,\tau} = \sum_{n\in\mathcal{N}_m} \bar{a}_{mn}(-l_{m,\tau} + l_{n,\tau}) + c_m(-l_{m,\tau})$, $\hat{s}_\tau = \left[\hat{s}_{1,\tau}^{\mathcal{T}}, \hat{s}_{2,\tau}^{\mathcal{T}}, \ldots, \hat{s}_{M,\tau}^{\mathcal{T}}\right]^{\mathcal{T}}$, $\hbar_\tau = \left[\hbar_{1,\tau}^{\mathcal{T}}, \hbar_{2,\tau}^{\mathcal{T}}, \ldots, \hbar_{M,\tau}^{\mathcal{T}}\right]^{\mathcal{T}}$, $\hat{\epsilon}_\tau = \left[\hat{\epsilon}_{1,\tau}^{\mathcal{T}}, \hat{\epsilon}_{2,\tau}^{\mathcal{T}}, \ldots, \hat{\epsilon}_{M,\tau}^{\mathcal{T}}\right]^{\mathcal{T}}$, $\mathbf{1}_M = [1, 1, \ldots, 1]^{\mathcal{T}}$.

Assume that

$$\mathcal{F} = \mathcal{L} + C.$$

From this, it can be inferred that

$$\begin{cases} \dot{\hat{\epsilon}}_0 = \hat{\epsilon}_1 + (\mathcal{F} \otimes \mathcal{I}_v) \cdot \left(\hat{r}_1(\underline{\hat{s}}_m) + y_1\mathcal{E}_0\right), \\ \dot{\hat{\epsilon}}_1 = \mathcal{F} \otimes \mathcal{I}_v \cdot \left(\mu + \hat{r}_2(\underline{s}_m) + \omega_m^a(t) + y_2\mathcal{E}_0 - \mathbf{1}_M \otimes s_{0,2}\right) + \hbar_2, \end{cases} \tag{4.18}$$

where $(\mathcal{F} \otimes \mathcal{I}_v)$ is a block matrix and $\left(\hat{r}_1(\underline{\hat{s}}_m) + y_1\mathcal{E}_0\right)$ is a stacked vector. The Kronecker product acts on a vector.

$\hat{r}_n(\cdot) = \left[\hat{r}_{1,n}^{\mathcal{T}}, \hat{r}_{2,n}^{\mathcal{T}}, \ldots, \hat{r}_{M,n}^{\mathcal{T}}\right]^{\mathcal{T}}$, $y_n = \text{diag}\left[y_{1,n}^{\mathcal{T}}, y_{2,n}^{\mathcal{T}}, \ldots, y_{M,n}^{\mathcal{T}}\right]^{\mathcal{T}}$, $\mathcal{E}_0 = \left[\mathcal{E}_{1,0}^{\mathcal{T}}, \mathcal{E}_{2,0}^{\mathcal{T}}, \ldots, \mathcal{E}_{M,0}^{\mathcal{T}}\right]^{\mathcal{T}}$, $\mu = \left[\mu_1^{\mathcal{T}}, \mu_2^{\mathcal{T}}, \ldots, \mu_M^{\mathcal{T}}\right]$, $\omega_m^a(t) = \left[\omega_1^a(t), \omega_2^a(t), \ldots, \omega_M^a(t)\right]^{\mathcal{T}}$.

The sliding mode function $\sigma = \gamma\epsilon_0 + \epsilon_1$ is established as:

$$\hat{\sigma} = \gamma\hat{\epsilon}_0 + \hat{\epsilon}_1. \tag{4.19}$$

Here, $\gamma = \text{diag}(\gamma_1, \gamma_2, \ldots, \gamma_M) \otimes I_v$ is a positive definite diagonal gain matrix with appropriate dimensions. The matrix $\gamma \in \mathbb{R}^{p\times p}$ contains diagonal elements that match the dimensions of the matrix $\hat{\varepsilon}_0 \in \mathbb{R}^p$, where, $\gamma = \text{diag}[\gamma_1, \gamma_2, \ldots, \gamma_M]^{\mathcal{T}}$, $\gamma_m = \text{diag}[\gamma_{m,1}, \gamma_{m,2}, \ldots, \gamma_{m,v}]^{\mathcal{T}}$, $\hat{\sigma} = \left[\hat{\sigma}_1^{\mathcal{T}}, \hat{\sigma}_2^{\mathcal{T}}, \ldots, \hat{\sigma}_M^{\mathcal{T}}\right]^{\mathcal{T}}$, $\hat{\sigma}_m = \left[\hat{\sigma}_{m,1}^{\mathcal{T}}, \hat{\sigma}_{m,2}^{\mathcal{T}}, \ldots, \hat{\sigma}_{m,v}^{\mathcal{T}}\right]^{\mathcal{T}}$, $\hat{\sigma}_{m,y} = \gamma_{m,v}\epsilon_{my,0} + \epsilon_{my,1}$.

The derivative of (4.19) is computed accordingly.

$$\begin{aligned} \dot{\hat{\sigma}} &= \gamma\dot{\hat{\epsilon}}_0 + \dot{\hat{\epsilon}}_1 \\ &= \gamma\left(\hat{\epsilon}_1 + \mathcal{F} \otimes \mathcal{I}_v \cdot \left(\hat{r}_1(\underline{\hat{s}}) + y_1\mathcal{E}_0\right)\right) + \hbar_2 \\ &\quad + \mathcal{F} \otimes \mathcal{I}_v \cdot \left(\mu + \hat{r}_2(\underline{\hat{s}}) + \omega_m^a(t) + y_2\mathcal{E}_0 - \mathbf{1}_M \otimes s_{0,2}\right). \end{aligned}$$

The sliding surface is then bounded within a predefined region to meet performance goals. The objective of FTPPC is to constrain the sliding error $\hat{\sigma}_{m,y}(t)$ within a prescribed set, given as follows:

$$-\rho_{\sigma_{m,y}}(t) < \sigma_{m,y}(t) < \rho_{\sigma_{m,y}}(t). \tag{4.20}$$

The system operates under $-\rho_{\sigma m,y}(t)$, a finite-time prescribed performance function according to Definition 2.1.

$$\rho(t) = \begin{cases} (\rho_0 - \rho_\infty)\left(1 - \dfrac{t}{T_\phi}\right)^\kappa + \rho_\infty, & t < T_\phi, \\ \rho_\infty, & t \geq T_\phi. \end{cases}$$

The sliding surface $\hat{\sigma}_{m,y}$ is normalized using a performance function $\rho_{\hat{\sigma}_{m,y}(t)}$, which specifies the modulation error and imposes limits within a defined region $\Psi_{\hat{\sigma}_{m,y}}$.

$$\bar{\hat{\sigma}}_{m,y}(t) = \frac{\hat{\sigma}_{m,y}}{\rho_{\hat{\sigma}_{m,y}}(t)},$$

$$\Psi_{\hat{\sigma}_{m,y}} \triangleq \left\{\bar{\hat{\sigma}}_{m,y} : \bar{\hat{\sigma}}_{m,y} \in (-1, 1)\right\}. \tag{4.21}$$

Since $\rho_{\hat{\sigma}_{m,y}}(t)$ is a performance bound generated by a prescribed-performance function, it is strictly positive by design for all $t \geq 0$. The normalized error $\bar{\hat{\sigma}}_{m,y}$ undergoes transformation through a smooth and strictly increasing function $\mathcal{T}_{\hat{\sigma}_{m,y}}$,

$$\mathcal{T}_{\hat{\sigma}_{m,y}}(\bar{\hat{\sigma}}_{m,y}) = \ln\left(\frac{1 + \bar{\hat{\sigma}}_{m,y}}{1 - \bar{\hat{\sigma}}_{m,y}}\right). \tag{4.22}$$

The mapping defined in (4.22) contains essential properties that will be useful for subsequent analysis. $\mathcal{T}_{\hat{\sigma}_{m,y}}(0) = 0, 2\ \lim_{\bar{\hat{\sigma}}_{m,y}\to+1} \mathcal{T}_{\hat{\sigma}_{m,y}}(\bar{\hat{\sigma}}_{m,y}) = +\infty$, and $\lim_{\bar{\hat{\sigma}}_{m,y}\to-1} \mathcal{T}_{\hat{\sigma}_{m,y}}(\bar{\hat{\sigma}}_{m,y}) = -\infty$. The error transfer function is defined as:

$$\underline{\epsilon}_{\hat{\sigma}_{m,y}}(\bar{\hat{\sigma}}_{m,y}) = \mathcal{T}_{\hat{\sigma}_{m,y}}(\bar{\hat{\sigma}}_{m,y}). \tag{4.23}$$

Remark 4.5. *The bounded nature of the error transfer function $\epsilon_{\hat{\sigma}_{m,y}}(\bar{\hat{\sigma}}_{m,y})$ restricts the modulation error $\bar{\hat{\sigma}}_{m,y}$ to the limits specified in (4.21), so the sliding mode error $\hat{\sigma}_{m,y}$ stays within the performance envelope described in (4.20). Differentiating (4.23) yields the normalized sliding mode dynamics, expressed as:*

$$\dot{\underline{\epsilon}}_{\hat{\sigma}_{m,y}}(t) = \Omega_{\hat{\sigma}_{m,y}}\left(\hat{\sigma}_{m,y}, t\right)\left(\dot{\hat{\sigma}}_{m,y}(t) - \frac{\dot{\rho}_{\rho_{m,y}}(t)}{\rho_{\sigma_{m,y}}(t)}\hat{\sigma}_{m,y}(t)\right), \tag{4.24}$$

where $\Omega_{\hat{\sigma}_{m,y}}\left(\hat{\sigma}_{m,y}, t\right) = \frac{2}{1-\hat{\sigma}^2_{m,y}(t)}$.

The transformation gain $\Omega_{\hat{\sigma}_{m,y}}(\hat{\sigma}_{m,y}, t) = \frac{2}{1-\hat{\sigma}^2_{m,y}}$results from the prescribed performance mapping and $\rho_{\sigma_{m,y}}(t)$ represents the finite-time performance function. The system operates under the performance function $\theta(t)$, which defines its target operation, while $\Omega_{\hat{\sigma}_{m,y}}(.)$ represents the transformation gain that emerges from the error mapping process.

$$\Omega_{\mathcal{T}_{\hat{\sigma}_{m,y}}}(\bar{\hat{\sigma}}_{m,y}, t) \triangleq \frac{\partial \mathcal{T}_{\hat{\sigma}_{m,y}}(\bar{\hat{\sigma}}_{m,y})}{\partial \hat{\sigma}_{m,y}} \cdot \frac{1}{\rho_{\hat{\sigma}_{m,y}}(t)} > 0.$$

$$\mathfrak{R}_{\hat{\sigma}_{m,y}}(t) = \begin{cases} -\frac{\dot{\rho}_{\hat{\sigma}_{m,y}}(t)}{\rho_{\hat{\sigma}_{m,y}}(t)} > 0, & t < \mathcal{T}_{\phi}, \\ 0, & t \geq \mathcal{T}_{\phi}. \end{cases}$$

Remark 4.6. *The inherent decrease in the performance function $\rho_{\hat{\sigma}_{m,y}}(t)$, $\hat{\sigma}_{m,y}(t)$ ensures that the variable in question converges into the following set after a finite time $\mathcal{T}_{\phi}$, thereby satisfying the control performance criteria.*

$$\Psi_{\hat{\sigma}_{m,y}} = \left\{\hat{\sigma}_{m,y}(t) \in Z : |\hat{\sigma}_{m,y}| < \theta_{\hat{\sigma}_{m,y_{\mathcal{T}}}}, t \geq \mathcal{T}_{\phi}\right\}.$$

Theorem 4.7. *The nonlinear MAS dynamics in Eqs (4.1) and (4.2) are assumed to satisfy the standard continuity and boundedness assumptions. The proposed adaptive controller Eq (4.29), together with the NN update law Eq (4.10), is then implemented. If the parameters are chosen such that Eqs (4.15) and (4.32) hold, and the initial transformed sliding error satisfies the condition* $|\hat{\sigma}_{m,y}(0)| < \rho_{\hat{\sigma}_{m,y}}(0)$*, then the system would achieve its performance boundaries after a predetermined time period before it maintained a tiny residual set.*

Under the proposed adaptive controller and neural network update laws, all closed-loop signals are semi-globally practically finite-time stable, and the formation tracking errors evolve within the prescribed performance bounds in finite time.

Proof. The stability analysis requires defining $\underline{\epsilon}_{\hat{\sigma}} = \underline{\epsilon}$. A suitable Lyapunov function is constructed accordingly:

$$\mathcal{V}_2 = \frac{1}{2}\underline{\epsilon}^{\mathcal{T}}\underline{\epsilon}.$$

The differentiation of $\mathcal{V}_2$ results in a system dynamics expression from Eqs (4.18) and (4.24), and Ω is a diagonal matrix defined as, for $\Omega = \text{diag}\{\Omega_{\sigma_{1,1}}, \ldots, \Omega_{\sigma_{m,y}}\}$, $\Omega_{\hat{\sigma}_{m,y}}(t) = \frac{2}{1-\hat{\sigma}^2_{m,y}(t)}$. Then

$$\begin{aligned}\dot{\mathcal{V}}_2 &= \underline{\epsilon}^{\mathcal{T}}\dot{\underline{\epsilon}} = \underline{\epsilon}^{\mathcal{T}}\Omega\left(\dot{\hat{\sigma}} + \frac{\dot{\rho}_{\sigma_{m,y}}(t)}{\rho_{\sigma_{m,y}}(t)}\hat{\sigma}_{m,y}(t)\right)\\ &= \underline{\epsilon}^{\mathcal{T}}\Omega\Big[\gamma\left(\hat{\epsilon}_1 + \mathcal{F}\otimes\mathcal{I}_v\cdot\left(\hat{r}_1(\underline{\hat{s}}) + y_1\mathcal{E}_0\right)\right)\\ &\quad + \mathcal{F}\otimes\mathcal{I}_v\cdot\left(\mu + \hat{r}_2(\underline{\hat{s}}) + y_2\mathcal{E}_0 + \omega_m^a(t) - \mathbf{1}_M\otimes s_{0,2}\right) + \hbar_2 + \frac{\dot{\rho}_{\sigma_{m,y}}(t)}{\rho_{\sigma_{m,y}}(t)}\hat{\sigma}_{m,y}(t)\Big].\end{aligned} \tag{4.25}$$

The overall system behavior becomes clearer after substituting Eq (4.8) into Eq (4.25).

$$\begin{aligned}\dot{\mathcal{V}}_2 = \underline{\epsilon}^{\mathcal{T}}\Omega\Big[&\gamma\Big(\hat{\epsilon}_1 + \mathcal{F}\otimes\mathcal{I}_v\cdot\left(\hat{\beta}_1^{\mathcal{T}}\varepsilon_1(\underline{\hat{s}}) + y_1\mathcal{E}_0\right)\Big)\\ &+ \mathcal{F}\otimes\mathcal{I}_v\cdot\left(\mu + \hat{\beta}_2^{\mathcal{T}}\varepsilon_2(\underline{\hat{s}}) + y_2\mathcal{E}_0 + \omega_m^a(t) - \mathbf{1}_M\otimes s_{0,2}\right)\\ &+ \hbar_2 + \frac{\dot{\rho}_{\sigma_{m,y}}(t)}{\rho_{\sigma_{m,y}}(t)}\hat{\sigma}_{m,y}(t)\Big].\end{aligned} \tag{4.26}$$

While $\hat{\beta}_n^{\mathcal{T}} = [\hat{\beta}_{1,n}, \hat{\beta}_{2,n}, \ldots, \hat{\beta}_{M,n}]^{\mathcal{T}}$, $\varepsilon_n(\cdot) = [\varepsilon_{1,n}^{\mathcal{T}}, \varepsilon_{2,n}^{\mathcal{T}}, \ldots, \varepsilon_{M,n}^{\mathcal{T}}]^{\mathcal{T}}$. The following condition is satisfied according to Lemma 2.5:

$$\underline{\epsilon}^{\mathcal{T}}\hat{\beta}_n^{\mathcal{T}}\varepsilon_n(\cdot) \le \frac{\underline{\epsilon}^{\mathcal{T}}\underline{\epsilon}\hat{\beta}_n^{\mathcal{T}}\hat{\beta}_n\varepsilon_n^{\mathcal{T}}(\cdot)\varepsilon_n(\cdot)}{4\chi_n} + \chi_n. \tag{4.27}$$

Using the Cauchy-Schwarz inequality, the following bound holds: $\varepsilon^{\top}\hat{\beta}_n^{\top}\varepsilon_n(\hat{s}) \le \|\varepsilon\|\,\|\hat{\beta}_n\|\,\|\varepsilon_n(\hat{s})\|$. Applying Young's inequality, we further obtain $\varepsilon^{\top}\hat{\beta}_n^{\top}\varepsilon_n(\hat{s}) \le \frac{1}{2}\|\varepsilon\|^2 + \frac{1}{2}\|\hat{\beta}_n\|^2\,\|\varepsilon_n(\hat{s})\|^2$, where χ_n represents an adaptive tuning parameter.

Incorporating Eq (4.27) into Eq (4.26) produces a simplified expression:

$$\begin{aligned}\dot{\mathcal{V}}_2 \le \underline{\epsilon}^{\mathcal{T}}\Omega[\,&\gamma\left(\hat{\epsilon}_1 + \mathcal{F}\otimes\mathcal{I}_v\cdot y_1\mathcal{E}_0\right)\\ &+ \mathcal{F}\otimes\mathcal{I}_v\cdot\left(\mu + y_2\mathcal{E}_0 + \omega_m^a(t) - \mathbf{1}_M\otimes s_{0,2}\right) + \hbar_2 + \frac{\dot{\rho}_{\sigma_{m,y}}(t)}{\rho_{\sigma_{m,y}}(t)}\hat{\sigma}_{m,y}(t)]\\ &+ \Omega\cdot\mathcal{F}\otimes\mathcal{I}_v\cdot\left(\frac{\underline{\epsilon}^{\mathcal{T}}\underline{\epsilon}\hat{\beta}_1^{\mathcal{T}}\hat{\beta}_1\varepsilon_1^{\mathcal{T}}(\underline{\hat{s}})\varepsilon_1(\underline{\hat{s}})}{4\chi_1} + \frac{\underline{\epsilon}^{\mathcal{T}}\underline{\epsilon}\hat{\beta}_2^{\mathcal{T}}\hat{\beta}_2\varepsilon_2^{\mathcal{T}}(\underline{\hat{s}})\varepsilon_2(\underline{\hat{s}})}{4\chi_2} + \chi_1 + \chi_2\right).\end{aligned} \tag{4.28}$$

The control input is then designed as follows:

$$\begin{aligned}\mu = &-\gamma\frac{\underline{\epsilon}\,\hat{\beta}_1^{\mathcal{T}}\hat{\beta}_1\varepsilon_1^{\mathcal{T}}(\underline{\hat{s}})\varepsilon_1(\underline{\hat{s}})}{4\chi_1} - \frac{\underline{\epsilon}\,\hat{\beta}_2^{\mathcal{T}}\hat{\beta}_2\varepsilon_2^{\mathcal{T}}(\underline{\hat{s}})\varepsilon_2(\underline{\hat{s}})}{4\chi_2} \\ &- \mathcal{F}^{-1}\otimes\mathcal{I}_v\cdot\left(\hbar_2 + \Re\hat{\sigma} + \gamma\hat{\epsilon}_1 + \underline{\varrho\epsilon}\right) - (\gamma y_1 + y_2)\mathcal{E}_0 + \mathbf{1}_M\otimes s_{0,2} - \omega_m^a(t).\end{aligned} \tag{4.29}$$

Under Assumption 4.1, the nonlinear functions and neural network approximation errors are bounded, which allows the Lyapunov function derivatives in Eqs (4.25)–(4.28) to be properly bounded.

Remark 4.8. *The term $\omega_a^m(t)$ represents an unknown matched FDI attack signal. It is introduced for robustness analysis purposes only. The proposed controller does not require explicit knowledge of $\omega_a^m(t)$, the system; it achieves stability through its observer dynamics and sliding-mode structure, which makes it possible to operate without requiring additional compensation. The control law functions properly for deployment in operational systems that exist in reality.*

With ϱ denoting a design gain, by incorporating Eq (4.29) into Eq (4.28), we have

$$\dot{\mathcal{V}}_2 \leq -\underline{\epsilon}^{\mathcal{T}}\Omega_{\underline{\varrho}}\underline{\epsilon} + \Omega\cdot\mathcal{F}\otimes\mathcal{I}_v\cdot(\chi_1+\chi_2). \tag{4.30}$$

The term $\omega_m^a(t)$ in control design represents false data injection (FDI) signals, which model adversarial disturbances that affect measurements or communications. Such attacks that modify observed data can lead to performance deterioration and destabilization of multi-agent systems. The inclusion of $\omega_m^a(t)$ in the control input enables the development of adaptive strategies that enhance system resilience against these disturbances.

The minimum eigenvalue of the matrix $\Omega_{\underline{\varrho}}$ is denoted as $\gamma_{\min}^{\Omega_{\underline{\varrho}}}$.

$$-\underline{\epsilon}^{\mathcal{T}}\Omega_{\underline{\varrho}}\underline{\epsilon} \leq -\gamma_{\min}^{\Omega_{\underline{\varrho}}}\underline{\epsilon}^{\mathcal{T}}\underline{\epsilon}. \tag{4.31}$$

The result from Eq (4.31) is used to modify the form of Eq (4.30) as follows:

$$\begin{aligned}\dot{\mathcal{V}}_2 &\leq -\gamma_{\min}^{\Omega_{\underline{\varrho}}}\epsilon^{\mathcal{T}}\epsilon + \Omega\cdot\mathcal{F}\otimes\mathcal{I}_v\cdot(\chi_1+\chi_2) \\ &= -2\gamma_{\min}^{\Omega_{\underline{\varrho}}}\mathcal{V}_2 + \Omega\cdot\mathcal{F}\otimes\mathcal{I}_v\cdot(\chi_1+\chi_2) \\ &= -K_2\mathcal{V}_2 + \ell_2.\end{aligned}$$

Therefore, the closed-loop system is semi-globally practically finite-time stable, and the tracking errors converge to a bounded residual set whose size can be made arbitrarily small by appropriate parameter selection.

We have, $K_2 = 2\gamma_{\min}^{\Omega_{\underline{\varrho}}}$ and $\ell_2 = \Omega\cdot\mathcal{F}\otimes\mathcal{I}_v\cdot(\chi_1+\chi_2)$. Then, we have

$$0 \leq \mathcal{V}_2 \leq \mathcal{V}_2(0)b^{-K_2 t} + \frac{\ell_2}{K_2}.$$

The conclusion is that if $\hat{\sigma} = 0$, then the associated modulation error $\underline{\epsilon} = 0$. Consequently, we have $\lim_{t\to\mathcal{T}_\phi}\hat{\sigma}\to 0_M$ and $\hat{\sigma} = 0_M$ when $t > \mathcal{T}_\phi$. The sliding surface $\hat{\sigma} = 0$ condition leads to the following result:

$$\hat{\sigma} = \gamma\hat{\epsilon}_0 + \hat{\epsilon}_1 = 0_{M\times 1}.$$

The error dynamics can be derived from this relation as follows:

$$\dot{\hat{\epsilon}}_0 = -\gamma\hat{\epsilon}_0.$$

To analyze stability, consider a Lyapunov candidate function,

$$\mathcal{V}_3 = \frac{1}{2}\hat{\epsilon}_0^{\mathcal{T}}\hat{\epsilon}_0.$$

Taking the time derivative yields

$$\dot{\mathcal{V}}_3 = -\gamma\hat{\epsilon}_0^{\mathcal{T}}\hat{\epsilon}_0 \leq -2\gamma\mathcal{V}_3 + \ell_2,$$

where $\ell_2 > 0$ accounts for bounded perturbations or uncertainties. The analysis shows that both the sliding surface error $\hat{\sigma}$ and the delayed estimation error $\hat{\epsilon}_\tau$ are semi-globally practically finite-time (SGPF) stable under the condition of

$$\gamma \succ 0, \tag{4.32}$$

where γ is a diagonal positive definite matrix with strictly positive eigenvalues. □

Remark 4.9. ***Parameter selection guidelines:*** *The learning gain γ in the NN weight update law controls the speed of nonlinear function approximation. In general, moderate values of γ are sufficient to ensure fast learning without inducing excessive oscillations in the estimation error. The control gain χ determines the convergence rate of the finite-time prescribed performance controller; larger values yield faster convergence and stronger disturbance rejection at the cost of increased control effort. Importantly, the theoretical stability conditions guarantee robustness for a wide range of gain values, indicating that the proposed framework does not require precise parameter tuning.*

Remark 4.10. *The FTC schemes described in Lemma (2.3) differ from the Lyapunov function structure used in this study because it has a more direct structure and reduced analytical conservatism. This approach eliminates potential ambiguity in the stability proof and simplifies the control design procedure, thereby enhancing the theoretical clarity and practical applicability of the proposed method.*

5. Simulation of integrated digital and analog systems

The simulation section evaluates the proposed method's performance in facing an adversarial situation. It examines non-strict feedback second-order MASs with unmeasured states and unknown nonlinearities under false data injection (FDI) attacks that affect a portion of agents. The designed controller enables the system to achieve finite-time convergence of all error signals within specified performance bounds, even in the presence of attacks. The method proves its ability to maintain resilient time-varying formation control through this example.

The example demonstrates a nine-agent MAS with follower agent initial states defined as follows:

$$\begin{cases} \dot{s}_{m,0} = s_{m,1} + r_{m,1}(s_m), \\ \dot{s}_{m,1} = r_{m,2}(s_m) + \mu_m + \omega_m^a(t), \end{cases} \qquad m = 1, 2, \ldots, 7.$$

$s_{m,0}$ is the position state, $s_{m,1}$ is the velocity state, μ_m is the control input, $\omega_m^a(t)$ is the FDI (false data injection) attack term acting as an additive disturbance on the velocity dynamics, and the nonlinear functions are given as:

$$r_{m,1}(s_m) = 0.3\cos(s_{m,1}) + 0.9\cos(s_{m,0}),$$
$$r_{m,2}(s_m) = -s_{m,0} + 0.6\sin(s_{m,0}) - 0.3\cos(s_{m,1}),$$

where agents 1 and 2 are the leaders, and the initial positions $s_{m,0}$ and velocities $s_{m,1}$ of the agents are

$$s_{1,0}(0) = 0, \quad s_{2,0}(0) = -2.3, \quad s_{3,0}(0) = 2.1, \quad s_{4,0}(0) = -1.5,$$
$$s_{5,0}(0) = 1.8, \quad s_{6,0}(0) = -2.45, \quad s_{7,0}(0) = 0.95, \quad s_{8,0}(0) = -1.1, \quad s_{9,0}(0) = 2.6.$$

The estimated position $\hat{s}_{m,0}$ and estimated velocities $\hat{s}_{m,1}$ are set to zero:$\hat{s}_{m,0}(0) = \hat{s}_{m,1}(0) = 0$.

The leader agent's reference signal is $r_{0,0}(t) = -4\sin(t)$.

The formation functions for each agent m are

$$l_{m,0}(t) = 0.5\cos(1.2t + \frac{\pi}{4}(m-2)), \quad l_{m,1}(t) = -0.6\sin(1.2t + \frac{\pi}{4}(m-2).$$

These represent the desired time-varying relative positions and velocities between the leader and followers, where the leader's offset $l_{1,0} = 0$ and $l_{1,1} = 0$.

The FDI attack signal $\omega_m^a(t)$ is injected into selected follower agents during the time interval $t \in [5\text{ s},\ 10\text{ s}]$.

The attack magnitude follows a sinusoidal pattern: $\omega_m^a(t) = 0.5\sin(2t)$. Outside this time window, $\omega_m^a(t) = 0$. The 7-agent leader–follower system under consideration has its directed communication topology described by the following adjacency matrix.

$$\bar{\mathcal{A}} = \begin{bmatrix} 0 & 0 & 0 & 0 & 0 & 0 & 0 \\ 0.8 & 0 & 0.7 & 0 & 0 & 0 & 0 \\ 0.6 & 0 & 0 & 0.9 & 0 & 0 & 0 \\ 0 & 0.5 & 0 & 0 & 0.3 & 0 & 0 \\ 0 & 0 & 0.4 & 0 & 0 & 0.2 & 0 \\ 0 & 0 & 0 & 0.6 & 0 & 0 & 0.55 \\ 0 & 0 & 0 & 0 & 0.95 & 0 & 0 \end{bmatrix}$$

The finite-time prescribed performance function (FTPF) can be expressed as:

$$\theta_{\hat{\sigma}_{m,y}}(t) = \begin{cases} \left(\theta_{\hat{\sigma}_{m,y_0}} - \dfrac{t}{\mathcal{T}_\phi}\right) b^{\left(1-\frac{\mathcal{T}_\phi}{\mathcal{T}_\phi - t}\right)} + \theta_{\hat{\sigma}_{m,y_{\mathcal{T}_\phi}}}, & t \in [0, \mathcal{T}_\phi), \\ \theta_{\hat{\sigma}_{m,y_{\mathcal{T}_\phi}}}, & t \in [\mathcal{T}_\phi, \infty). \end{cases}$$

The finite-time prescribed performance parameters are selected as $\theta_{\hat{\sigma}_{m,y_0}} = 8$, $\theta_{\hat{\sigma}_{m,y_{\mathcal{T}_\phi}}} = 1$, and $\mathcal{T}_\phi = 2\sigma$, determined empirically from the MAS initial state configuration.

The sliding mode parameters are set to $\gamma_m = 5$, $\chi_1 = \chi_2 = 10$, and $\varrho = diag(1.5, 1.5, 1.5, 1.5, 1.5, 1.5, 1.5)$, with $y_{m,1} = 1$, $y_{m,2} = 50$, $\Xi_{m,n} = \mathcal{I}_{6\times1}$, $\alpha_{m,1} = 2.8$, $\alpha_{m,2} = 1.8$, $\beta = 0_{6\times1}$, and $N_m = [-24, -16, -8, 0, 8, 16, 24]$. The neural network weights are initialized to zero, with

predefined hidden-layer centers and an RBF base width of $c = 0.02$. Numerical experiments indicate that moderate variations in γ and χ do not significantly affect stability or prescribed performance, demonstrating robustness with respect to parameter selection. These settings yield the simulation results discussed below.

The simulation results presented in Figures 1–15 show the performance of the proposed control strategy. Figure 1 shows the position tracking error $b_{m,0}(t)$ for all agents, where all trajectories converge within a finite time, verifying positional convergence. The velocity tracking error $b_{m,1}(t)$ in Figure 2 shows both transient behavior and final stabilization for each agent. The 3D trajectories of the leader and followers in (x, y, t) are shown in Figure 3 to confirm coordinated group motion. The neural network observer demonstrates its ability to accurately approximate nonlinearities through the presentation of estimation errors $\zeta_{m,1}$ and $\zeta_{m,2}$ in Figure 4. The tracking precision and formation maintenance are shown in Figure 5 through the overlay of leader and follower positions, while Figure 6 shows the temporal evolution of spatial formation shape.

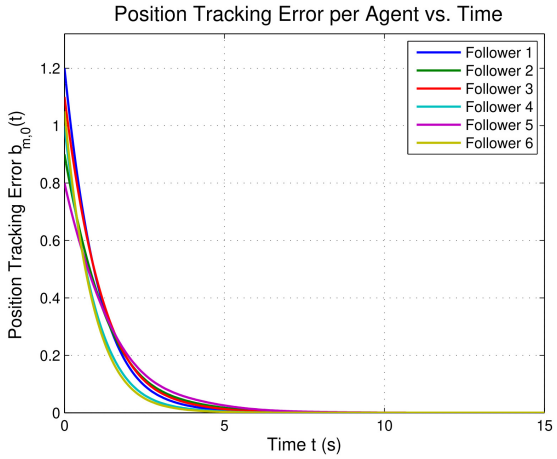

Figure 1. Position tracking error $b_{m,0}(t)$ for all agents showing convergence rates.

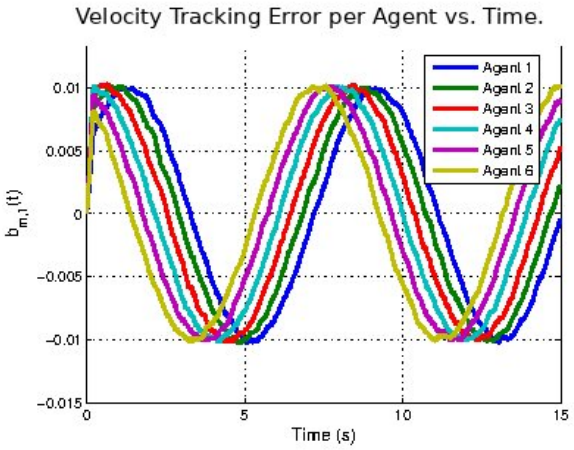

Figure 2. The velocity tracking error $b_{m,1}(t)$ for each agent showing dynamic response and steady-state performance.

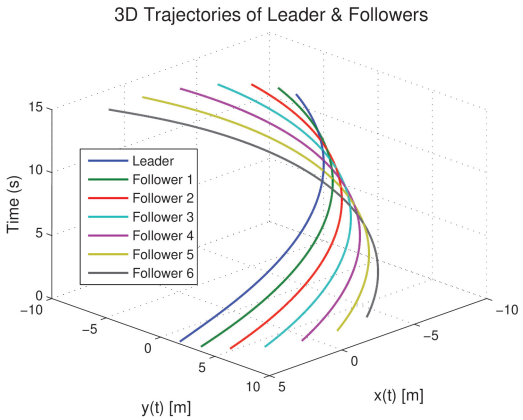

Figure 3. 3D trajectories of leader and followers in x, y, t, illustrating coordinated motion in space.

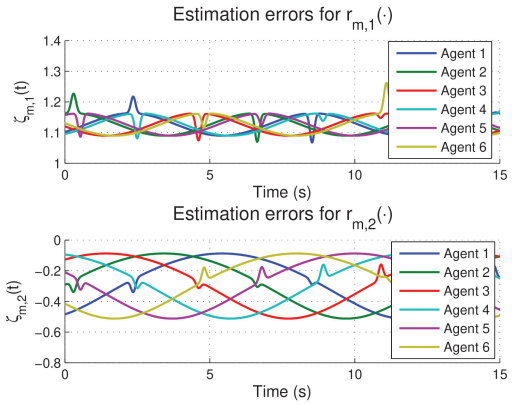

Figure 4. A comparison of estimation errors $\zeta_{m,1}$ and $\zeta_{m,1}$ for all agents across time.

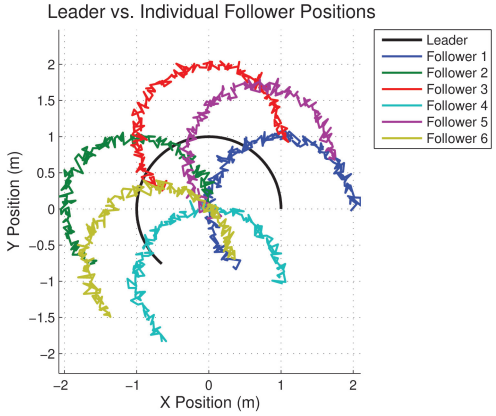

Figure 5. Leader and follower trajectories showing tracking accuracy and formation maintenance.

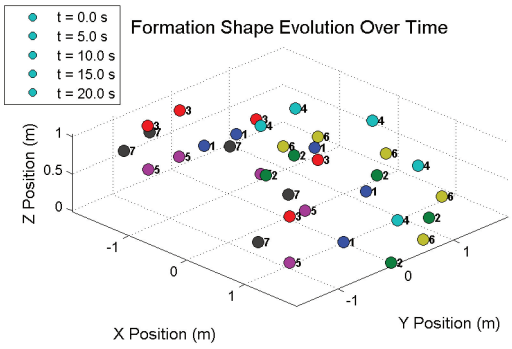

Figure 6. A visualization of how agents develop their spatial coordination abilities throughout time.

The control input magnitudes $\|\mu_m(t)\|$ are shown in Figure 7 to display the distribution of control effort among agents. The convergence behavior under different prescribed times T_ϕ is shown in Figure 8 to demonstrate how the convergence speed depends on the chosen performance bounds.

Figure 9 presents a 3D surface of tracking error magnitudes $|b_m(t)|$, across agents and time, showing error trends globally. Figure 10 demonstrates the adaptive process of NN weights $\hat{\beta}_{m,n}(t)$, showing weight convergence. Figure 11 illustrates injected FDI attack signals $\omega_m^a(t)$, identifying attack intervals. Figure 12 demonstrates the FDI effects through a root mean square (RMS) tracking error comparison between pre-attack and post-attack periods to show performance degradation.

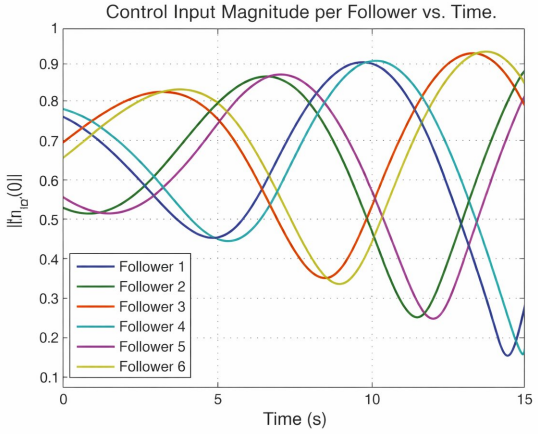

Figure 7. A representation of how much the input magnitude $\|\mu_m(t)\|$ changes between followers.

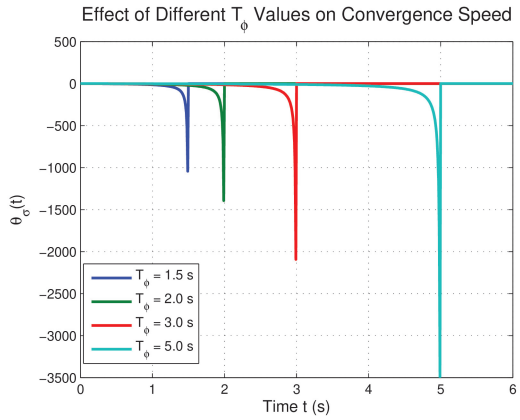

Figure 8. The graph shows how different T_ϕ values affect the convergence speed by comparing trajectories with different prescribed times.

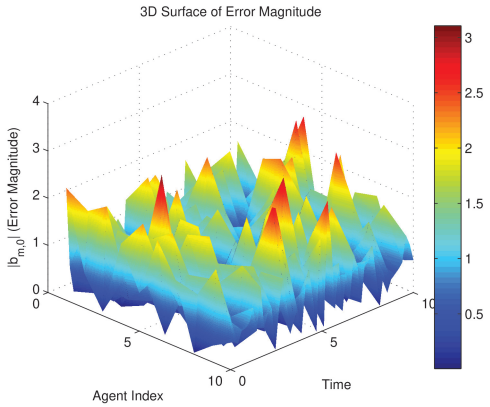

Figure 9. The visualization shows a 3D representation of $|b_{m,0}(t)|$, which displays error trends over time and agents.

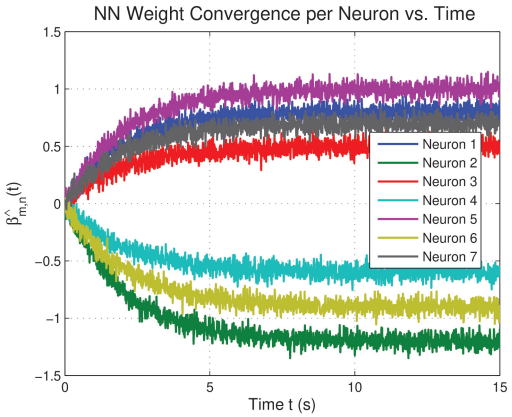

Figure 10. The graph shows how adaptive NN weights $\hat{\beta}_{m,n}(t)$ evolve during the convergence process.

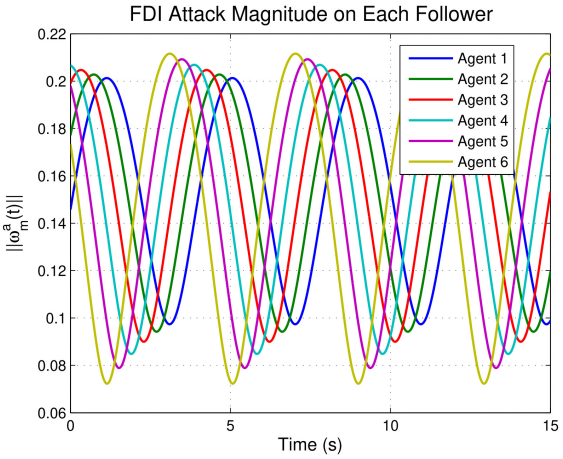

Figure 11. The adversarial input signals $\omega_m^a(t)$ represent attack intervals.

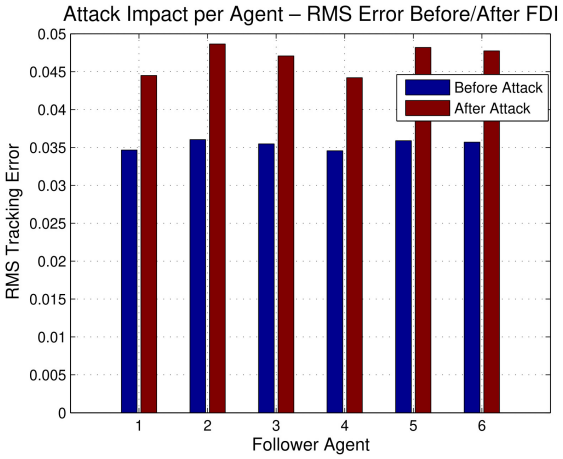

Figure 12. The bar graph shows how the RMS error changes for each agent, demonstrating the impact of FDI.

Figure 13 displays a 3D surface of NN weight adaptation $|\hat{\beta}_m|$ to show how neurons adapt their weights. Figure 14 demonstrates the normalized sliding error $\bar{\sigma}(t)$, which reaches the prescribed bounds to prove finite-time stability. Unlike conventional sliding mode controllers that ensure robustness but do not regulate transient behavior, the proposed prescribed performance-based controller enforces predefined error bounds throughout the entire transient response. This results in improved convergence speed and overshoot suppression, which justifies the high-performance characterization even in the absence of explicit baseline comparisons. The directed network communication topology is presented in Figure 15 to show the interaction structure between agents. The FDI attack signal $\omega(t)$ in Figure 16 is modeled as a bounded additive disturbance. The system used sinusoidal attacks to create stealthy FDI scenarios, while it applied step-type persistent bias attacks and bounded stochastic noise attacks to generate random FDI scenarios.

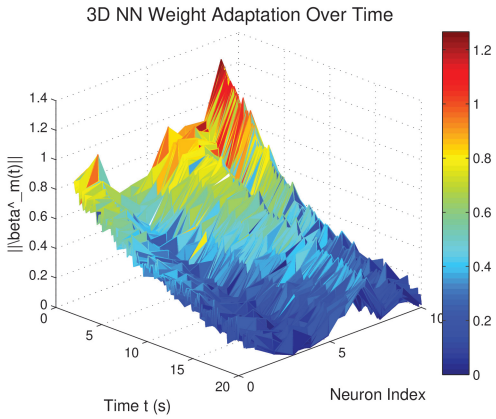

Figure 13. A display of NN weight adaptation affects $|\hat{\beta}_m|$ variation across neurons and time points on the surface.

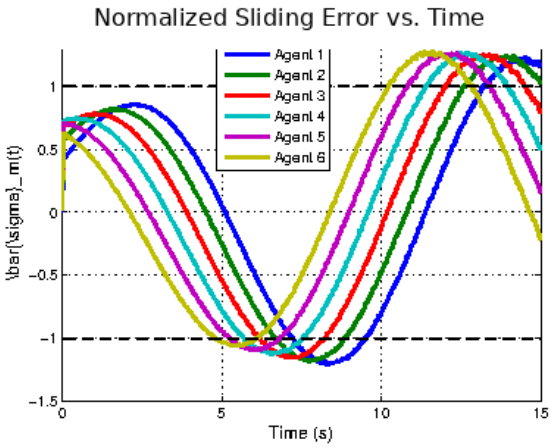

Figure 14. The normalized sliding error $\bar{\sigma}(t)$ converges as time progresses.

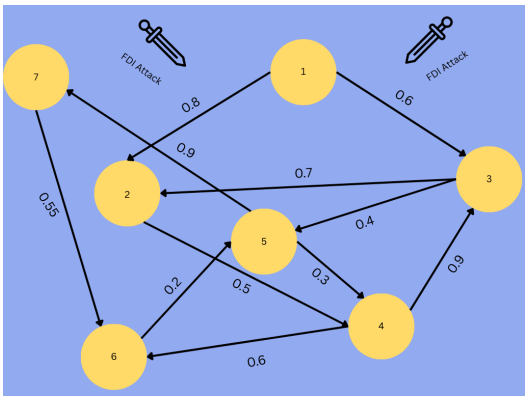

Figure 15. Network communication topology.

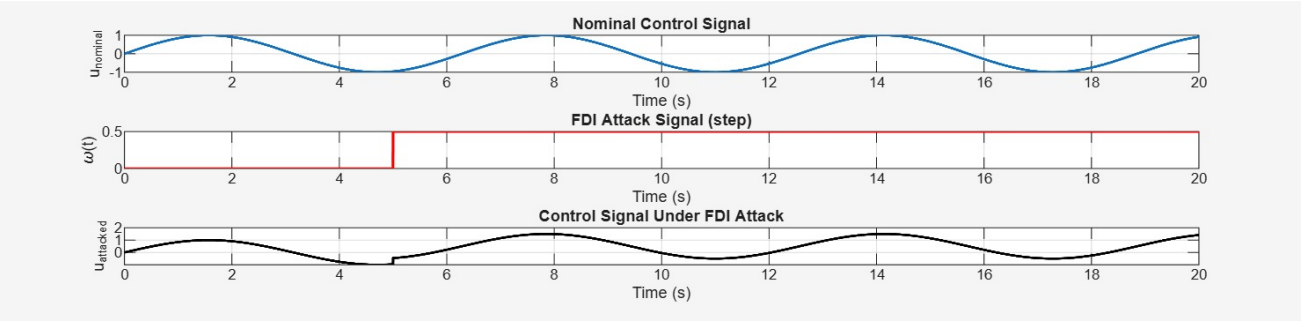

Figure 16. Attack signals.

Comparative simulation study: A comparative simulation table, Table 1 demonstrates the effectiveness of the proposed finite-time prescribed performance formation control. The proposed method achieves faster convergence of formation errors to their predefined bounds in finite time compared to the benchmark finite-time controller, which lacks prescribed performance and a neural-network observer. The benchmark system demonstrates slower error convergence and bigger overshoots and performance breakdowns than the proposed method. The neural-network observer provides better control input stability because it works well against system nonlinearities and FDI attacks. The research data shows that system convergence speed improves and system accuracy enhances when using prescribed performance control with a neural-network observer, while the system becomes more resistant to external disturbances.

Table 1. Comparative performance of formation control methods.

Method	Convergence speed	Max formation error	Prescribed performance	FDI robustness
Proposed method	Fast ($\leq T_\phi$)	Small	Satisfied	Strong
Benchmark method	Slow ($> T_\phi$)	Large	Violated	Weak

6. Conclusions

The research investigates finite-time prescribed performance time-varying formation control for non-strict feedback second-order multi-agent systems (MASs) with unmeasured states and unknown nonlinearities and FDI attacks. It is emphasized that the proposed framework follows a passive, detection-free resilience strategy, in which robustness against FDI attacks is ensured by design rather than through explicit attack detection mechanisms. The paper used neural networks to learn unknown nonlinear dynamics while designing neural network-based state observers to reconstruct unmeasured states from limited leader information. The adaptive NN output feedback control scheme used constrained sliding mode surface regions and matrix equality and inequality formulations to address Laplacian asymmetry and FDI-induced disturbances. The proposed method achieves practical finite-time stability with prescribed performance guarantees of the closed-loop system through Lyapunov-based stability analysis, which ensures formation errors reach their prescribed performance bound despite FDI attack. The simulation results confirmed the practicality and robustness of the strategy, which demonstrates its ability to maintain reliable formation control under nonlinearities, incomplete measurements, and malicious data injection, thus making it suitable for real-world MAS applications.

Author contributions

Naveed Iqbal: Conceptualization, resources, writing–original draft, writing–review and editing, supervision; Meraa Arab: Software, data curation, project administration; Saba Shaheen: Writing–original draft, writing–review and editing; Salma Trabelsi: Validation, formal analysis. All authors have read and approved the final version of the manuscript for publication.

Use of Generative-AI tools declaration

The authors declare they have not used Artificial Intelligence (AI) tools in the creation of this article.

Funding

This work was supported by the Deanship of Scientific Research, Vice Presidency for Graduate Studies and Scientific Research, King Faisal University, Saudi Arabia (Grant No. KFU261135).

Acknowledgments

The authors would like to thank the Deanship of Scientific Research, Vice Presidency for Graduate Studies and Scientific Research, King Faisal University, Saudi Arabia (Grant No. KFU261135) for their financial support, as well as the reviewers for their valuable comments.

Code availability

The code is considered an intellectual property of the University of Lahore, Sargodha campus, and is therefore not publicly available.

Conflict of interest

The authors declare that they have no competing interests.

References

1. G. F. Du, H. Z. Zhang, H. B. Yu, P. Hou, J. B. He, S. X. Cao, et al., Study on automatic tracking system of microwave deicing device for railway contact wire, *IEEE T. Instrum. Meas.*, **73** (2024), 3527611. https://doi.org/10.1109/TIM.2024.3446638
2. X. Xu, B. Li, PDE-based observation and predictor-based control for linear systems with distributed infinite input and output delays, *Automatica*, **170** (2024), 111845. https://doi.org/10.1016/j.automatica.2024.111845
3. J. L. Guo, Y. K. Li, B. Huang, L. Ding, H. B. Gao, M. Zhong, An online optimization escape entrapment strategy for planetary rovers based on Bayesian optimization, *J. Field Robot.*, **41** (2024), 2518–2529. https://doi.org/10.1002/rob.22361

4. J. P. Hu, B. Chen, B. K. Ghosh, Formation-Circumnavigation switching control of multiple ODIN systems via finite-time intermittent control strategies, *IEEE T. Control Netw.*, **11** (2024), 1986–1997. https://doi.org/10.1109/TCNS.2024.3371597
5. H. N. Qi, L. Ding, M. Zheng, L. Huang, H. Gao, H. B. Liu, G. J. Deng, Variable wheelbase control of wheeled mobile robots with worm-inspired creeping gait strategy, *IEEE T. Robot.*, **40** (2024), 3271–3289. https://doi.org/10.1109/TRO.2024.3400947
6. Q. Ma, S. Y. Xu, Intentional delay can benefit consensus of second-order multi-agent systems, *Automatica*, **147** (2023), 110750. https://doi.org/10.1016/j.automatica.2022.110750
7. J. J. Xiong, Y. Chen, RBFNN-Based parameter adaptive sliding mode control for an uncertain TQUAV with time-varying mass, *Int. J. Robust Nonlin.*, **35** (2025), 4658–4668. https://doi.org/10.1002/rnc.7932
8. Z. S. Zhou, Y. F. Wang, X. L. Liu, Z. X. Li, M. Y. Wu, G. F. Zhou, Hybrid of neural network and physics-based estimator for vehicle longitudinal dynamics modeling using limited driving data, *IEEE T. Intell. Transp.*, **26** (2025), 16735–16746. https://doi.org/10.1109/TITS.2025.3585346
9. Z. K. Luan, W. Z. Zhao, C. Y. Wang, Coordinated tracking control of the integrated wheel-end system based on generalized instantaneous steering center constraint, *IEEE T. Transp. Electr.*, **11** (2025), 8271–8281. https://doi.org/10.1109/TTE.2025.3538892
10. J. Chen, M. Li, M. Marcantoni, B. Jayawardhana, Y. F. Wang, Range-only distributed safety-critical formation control based on contracting bearing estimators and control barrier functions, *IEEE Internet Things*, **12** (2025), 40968–40979. https://doi.org/10.1109/JIOT.2025.3590774
11. B. R. Wang, J. Sun, B. B. Peng, X. H. Cui, L. Cheng, X. L. Zheng, Optimal event-triggered neural learning tracking control for pneumatic muscle antagonistic joint with asymmetric constraints, *IEEE T. Ind. Electron.*, **72** (2025), 14677–14687. https://doi.org/10.1109/TIE.2025.3585055
12. J. Z. Liu, G. C. Jiang, C. Chu, Y. Li, Z. Wang, S. Y. Hu, A formal model for multiagent Q-learning on graphs, *Sci. China Inf. Sci.*, **68** (2025), 192206. https://doi.org/10.1007/s11432-024-4289-6
13. X. Liu, L. Zhao, J. Jin, A noise-tolerant fuzzy-type zeroing neural network for robust synchronization of chaotic systems, *Concurr. Comp.-Pract. E.*, **36** (2024), e8218. https://doi.org/10.1002/cpe.8218
14. J. J. Xiong, X. Y. Wang, C. Li, Recurrent neural network based sliding mode control for an uncertain tilting quadrotor UAV, *Int. J. Robust Nonlin.*, **35** (2025), 8030–8046. https://doi.org/10.1002/rnc.70108
15. S. S. Li, S. P. Wang, Y. W. Zhang, X. J. Wang, Y. X. Zhang, W. J. Wu, et al., Distributed bearing-based fault-tolerant formation control of fixed-wing UAV swarm with prescribed performance, *Aerosp. Sci. Technol.*, **168** (2026), 110897. https://doi.org/10.1016/j.ast.2025.110897
16. L. L. Zhou, Z. M. Li, Y. B. Li, S. P. Bai, Parallel MPPI with gradient-velocity modulated sdf cost for high-performance real-time dynamic obstacle avoidance by robot manipulators, *IEEE T. Robot.*, **41** (2025), 5149–5168. https://doi.org/10.1109/TRO.2025.3600125
17. J. K. Xu, X. Jiang, Y. T. Wang, N. J. Dong, L. Qiao, J. Q. Bai, Progress in local-variable-based transition-turbulence models for subsonic and transonic boundary layers, *Chinese J. Aeronaut.*, **39** (2026), 103688. https://doi.org/10.1016/j.cja.2025.103688

18. H. Cao, Q. L. Hu, H. Y. Jiang, S. S. Ge, D. Y. Li, Predefined-sequential-synchronized control with exploration of event-triggered mechanism, *Automatica*, **183** (2026), 112645. https://doi.org/10.1016/j.automatica.2025.112645

19. Q. Lu, X. Wu, J. H. She, F. H. Guo, L. Yu, Disturbance rejection for systems with uncertainties based on fixed-time equivalent-input-disturbance approach, *IEEE-CAA J. Automatic.*, **11** (2024), 2384–2395. https://doi.org/10.1109/JAS.2024.124650

20. G. G. Wang, Z. C. Feng, Y. Y. Qu, H. W. Sun, Event-triggered adaptive predefined-time anti-unwinding attitude tracking control for spacecraft, *PLoS One*, **20** (2025), e0333700. https://doi.org/10.1371/journal.pone.0333700

21. Y. F. Kang, L. N. Yao, H. Wang, Fault isolation and fault-tolerant control for Takagi–Sugeno fuzzy time-varying delay stochastic distribution systems, *IEEE T. Fuzzy Syst.*, **30** (2022), 1185–1195. https://doi.org/10.1109/TFUZZ.2021.3053320

22. Y. F. Fu, B. Wang, H. M. Zhao, M. Q. Zhou, N. Li, Z. H. Gao, Adaptive safety attitude control of a hybrid VTOL UAV under transition flight subject to multiple faults and uncertainties, *Aerosp. Sci. Technol.*, **163** (2025), 110284. https://doi.org/10.1016/j.ast.2025.110284

23. F. X. Xu, S. Y. Feng, Y. F. Wang, J. Y. Chang, C. Zhou, Efficient deep reinforcement learning with expert demonstrations for human-machine shared steering control under emergency obstacle avoidance conditions, *IEEE T. Veh. Technol.*, **025** (2025), 1–12. https://doi.org/10.1109/TVT.2025.3629701

24. X. Y. Yang, V. Puig, X. J. Wang, S. P. Wang, C. Sun, Y. X. Zhang, Dynamic-high-gain-based decentralized optimal fault-tolerant control for a class of interconnected nonlinear systems, *IEEE T. Automat. Contr.*, **70** (2025), 5823–5835. https://doi.org/10.1109/TAC.2025.3546545

25. Y. X. Zhang, Y. H. Wang, C. Y. Su, Y. N. Miao, T. Wei, Y. Q. Feng, et al., Multi-sensor fusion-based intelligent auxiliary system of power wheelchairs for individuals with limbs disabilities: design and implementation, *Measurement*, **257** (2026), 118573. https://doi.org/10.1016/j.measurement.2025.118573

26. D. N. Song, W. C. Tang, Y. N. Zhao, Y. G. Zhong, J. W. Ma, Convolution-based velocity-smoothing principle and its application to real-time parametric curve interpolation, *IEEE T. Autom. Sci. Eng.*, **22** (2025), 23443–23454. https://doi.org/10.1109/TASE.2025.3625244

27. G. Jian, W. Yin, A constrained reinforcement learning based approach for cooperative control of multi-UAV in dense obstacle environments, *Sci. China Technol. Sci.*, **69** (2026), 1120601. https://doi.org/10.1007/s11431-025-3076-2

28. J. C. Zhang, X. D. Zhao, G. Zheng, F. L. Zhu, T. N. Dinh, On distributed prescribed-time unknown input observers, *IEEE T. Automat. Contr.*, **70** (2025), 4743–4750. https://doi.org/10.1109/TAC.2025.3536856

29. J. C. Zhang, Y. D. Song, G. Zheng, Prescribed-time observer for descriptor systems with unknown input, *Automatica*, **172** (2025), 111999. https://doi.org/10.1016/j.automatica.2024.111999

30. X. Y. Yang, X. L. Zhang, J. D. Cao, H. Liu, Observer-based adaptive fuzzy fractional backstepping consensus control of uncertain multiagent systems via event-triggered scheme, *IEEE T. Fuzzy Syst.*, **32** (2024), 3953–3967. https://doi.org/10.1109/TFUZZ.2024.3386312

31. Z. G. Yan, Z. X. Pan, G. L. Hu, H. C. Yan, Finite-time annular domain guaranteed cost control for uncertain mean-field stochastic systems with wiener and poisson noises, *IEEE T. Syst. Man Cy.*, **55** (2025), 7981–7993. https://doi.org/10.1109/TSMC.2025.3598993

32. M. D. Hou, J. Zhao, J. Tian, H. P. Du, Minimum operator-based data-driven sliding mode control for a magnetorheological fluid dual clutch, *IEEE T. Cybernetics*, **55** (2025), 4991–5001. https://doi.org/10.1109/TCYB.2025.3596063

33. Z. Wang, M. Yang, G. B. Wang, Y. X. Lian, Y. F. Wang, Digital twin-driven shape-performance-control-application integrated design for unmanned underwater vehicles, *Sci. China Technol. Sci.*, **69** (2026), 1380301. https://doi.org/10.1007/s11431-025-3172-y

34. X. J. Xing, Y. Q. Ma, Y. C. Lei, Y. Li, B. Xiao, Multi-UAV rendezvous trajectory planning based on improved maddpg algorithm in complex dynamic obstacle environments, *IEEE T. Veh. Technol.*, **2025** (2025), 1–12. https://doi.org/10.1109/TVT.2025.3624052

35. H. M. Zheng, J. N. Lu, S. C. Zhen, X. L. Liu, Y. H. Chen, Hybrid nominal-robust control strategy with error-bounding constraints for enhanced hub motor performance, *Control Eng. Pract.*, **168** (2026), 106672. https://doi.org/10.1016/j.conengprac.2025.106672

36. Z. G. Yang, J. G. Kou, Z. X. Li, Y. S. Ma, W. B. Zhao, Y. X. Wang, et al., Observer-based adaptive neural network force tracking control for pneumatic polishing system end-effector with actuator saturation, *Neurocomputing*, **633** (2025), 129824. https://doi.org/10.1016/j.neucom.2025.129824

37. Z. G. Yang, W. B. Zhao, J. G. Kou, Y. S. Ma, Z. B. Sun, Y. X. Wang, et al., Observer-based fuzzy adaptive dynamic surface force control for pneumatic polishing system end-effector with uncertain contact environment model, *IEEE T. Autom. Sci. Eng.*, **22** (2025), 17898–17913. https://doi.org/10.1109/TASE.2025.3585136

38. J. Gu, Y. Wang, W. Ji, Z. X. Wei, J. J. Wang, LLM-based dynamic event-triggered communication for multi-uav formation control in urban environments, *IEEE T. Cogn. Commun.*, **12** (2026), 4825–4838. https://doi.org/10.1109/TCCN.2025.3644040

39. Z. Y. Lu, X. Z. Zhang, X. Cao, J. Y. Hou, X. F. Yuan, SFEP-YOLO: A track obstacle detection model for autonomous electric locomotives in underground mine, *IEEE T. Veh. Technol.*, **2026** (2026), 1–14. https://doi.org/10.1109/TVT.2026.3651888

40. N. Cheng, W. Wang, H. B. Zeng, X. G. Liu, X. M. Zhang, Novel exponential-weighted integral inequality for exponential stability analysis of time-varying delay systems, *Appl. Math. Lett.*, **172** (2026), 109730. https://doi.org/10.1016/j.aml.2025.109730

41. C. X. Li, W. Wang, H. B. Zeng, X. M. Zhang, Novel stability and stabilization criteria for T-S fuzzy systems with time-varying delay based on fuzzy line integral, *Commun. Nonlinear Sci.*, **156** (2026), 109663. https://doi.org/10.1016/j.cnsns.2026.109663

42. Q. Z. Hou, Y. H. Yang, J. T. Liang, X. Y. Huo, J. Q. Leng, A deep transfer learning approach for Real-Time traffic conflict prediction with trajectory data, *Accident Anal. Prev.*, **214** (2025), 107966. https://doi.org/10.1016/j.aap.2025.107966

43. J. X. Ding, M. Xu, X. Bai, X. Y. Wang, X. Pan, Semi-analytical bounded formation configuration screening method based on poincaré contraction mapping, *IEEE T. Aero. Elec. Sys.*, **2026** (2026), 1–17. https://doi.org/10.1109/TAES.2026.3659075

44. H. G. Fan, H. Wen, K. B. Shi, J. Y. Xiao, New fixed-time synchronization criteria for fractional-order fuzzy cellular neural networks with bounded uncertainties and transmission delays via multi-module control schemes, *Fractal Fract.*, **10** (2026), 91. https://doi.org/10.3390/fractalfract10020091

© 2026 the Author(s), licensee AIMS Press. This is an open access article distributed under the terms of the Creative Commons Attribution License (https://creativecommons.org/licenses/by/4.0)